W-Band FMCW Radar for Range Finding, Static Clutter Suppression & Moving Target Characterization

by

Levi Tanner Goodman
B.S.E.E., Brigham Young University, 2016

Submitted to the graduate degree program in Electrical Engineering and Computer Science and the Graduate Faculty of the University of Kansas in partial fulfillment of the requirements for the degree of Master of Science.

_____

Chair: Christopher Allen

_____

Shannon Blunt

_____

James Stiles

Date Defended: 19 August 2019

The thesis committee for Levi Goodman
certifies that this is the approved version of the following thesis:

W-Band FMCW Radar for Range Finding, Static Clutter Suppression & Moving Target Characterization

_____

Chair: Christopher Allen

Date Approved: 30 August 2019

Abstract

Many radar applications today require accurate, real-time, unambiguous measurement of target range and radial velocity. Obstacles that frequently prevent target detection are the presence of noise and backscatter from other objects, referred to as clutter.

In this thesis, a method of static clutter suppression is proposed to increase detectability of moving targets in high clutter environments. An experimental dual-purpose, single-mode, monostatic FMCW radar, operating at 108 GHz, is used to map the range of stationary targets and determine range and velocity of moving targets. By transmitting a triangular waveform, which consists of alternating upchirps and downchirps, the received echo signals can be separated into two complementary data sets, an upchirp data set and a downchirp data set. In one data set, the return signals from moving targets are spectrally isolated (separated in frequency) from static clutter return signals. The static clutter signals in that first data set are then used to suppress the static clutter in the second data set, greatly improving detectability of moving targets. Once the moving target signals are recovered from each data set, they are then used to solve for target range and velocity simultaneously.

The moving target of interest for tests performed was a reusable paintball (reball). Reball range and velocity were accurately measured at distances up to 5 meters and at speeds greater than 90 m/s (200 mph) with a deceleration of approximately 0.155 m/s/ms (meters per second per millisecond). Static clutter suppression of up to 25 dB was achieved, while moving target signals only suffered a loss of about 3 dB.

Acknowledgements

I would like to thank Jeff Redmond, for his machining work on the frame of the radar system and for his input on component layout, Alex Griffin, for automating portions of the radar start-up process and synchronizing the digital synthesizers, and Lyndi Hanson for assisting in acquiring the paintball gun and associated hardware from the ROTC program at KU which was used for testing the detection of high-velocity targets.

Special thanks to Dr. Christopher Allen for his constant support over the last two years, and for his patience and time spent answering questions which helped me gain the knowledge and understanding necessary to finish this project.

This work is supported by the US Army Research Laboratory under contract number W911NF-16-2-0222.

Table of Contents

Chapter 1. Introduction 1

Chapter 2. System Design and Signal Progression 3

Chapter 3. Stretch Processing 11

Beat Frequency 11

3 MHz Offset 17

Chapter 4. Test Setup & Results 23

Test Procedure & Data Processing 23

Static Target Range Finding and Radar Calibration 25

Target Velocity Test Setup & Results 29

Chapter 5. Measuring Moving Target Range & Velocity 35

Chapter 6. Static Clutter Suppression 50

Spectral Isolation 50

Static Clutter Suppression 52

Chapter 7. Conclusion 62

References 64

APPENDIX A 65

APPENDIX B 69

APPENDIX C 70

List of Figures

Figure 2-1: Component level block diagram of Radar System 3

Figure 2-2: 430 MHz DDS output & 3rd Nyquist Zone image 6

Figure 2-3: ADRF6780 mixer output with and without filter 8

Figure 2-4: Final 18.08 GHz signal before passing through x6 multiplier 9

Figure 3-1: Calculating beat frequency using a sawtooth waveform 12

Figure 3-2: Obtaining beat frequency by mixing received and reference signals 14

Figure 3-3: Calculating beat frequency using a triangular waveform 16

Figure 3-4: Beat frequency obtained with no frequency offset 18

Figure 3-5: Interference generated in Receiver/Mixer/Multiplier chain 19

Figure 3-6: Beat frequency obtained with 3 MHz frequency offset 21

Figure 4-1: Unprocessed signal data overlaid with the DDS trigger signal. 24

Figure 4-2: Received signal data separated into upchirp and downchirp data sets 25

Figure 4-3: Stationary target ranging test setup 26

Figure 4-4: June 5 NSF2 upchirp/downchirp static target beat frequency symmetry 27

Figure 4-5: Osilloscope remote trigger system diagram 30

Figure 4-6: CW mode test setup for measuring target velocity 32

Figure 4-7: Reball Doppler frequency obtained while operating in CW mode 33

Figure 5-1: Aug 16 SFA4 surface plots. 35

Figure 5-2: Aug 16 SFA4 frequency spectrum 37

Figure 5-3: Aug 16 SFA4 reball upchirp/downchirp beat frequency comparison 38

Figure 5-4: Aug 16 SFA4 reball beat frequency vector indices 39

Figure 5-5: Aug 16 SFA4 upchirp/downchirp reball beat frequency interpolation 42

Figure 5-6: Aug 16 SFA4 reball range and velocity 45

Figure 5-7: Aug 16 SFA4 beat frequency/Doppler frequency with trendlines 47

Figure 6-1: Spectral Isolation MATLAB simulation. 51

Figure 6-2: Illustration of upchirp and downchirp signals for static and moving targets 53

Figure 6-3: Illustration of upchirp/downchirp signals after separation into two data sets 54

Figure 6-4: Illustration of clutter suppression process 55

Figure 6-5: Sep 6 SFA6 reball signal in clutter-heavy environment 57

Figure 6-6: Sep 6 SFA6 pre-suppression range & velocity 58

Figure 6-7: Sep 6 SFA6 post-suppression range & velocity 59

Figure 6-8: Sep 6 SFA6 beat frequency & Doppler frequency as a function of time 60

Figure 6-9: Sep 6 SFA6 range & velocity real-time vs post-processing comparison 61

List of tables

Table 2-1: Radar system component names, symbols, and descriptions 4

Table 4-1: Reball firing data comparison for CW mode operation 34

Chapter 1. Introduction

Radar systems have been used for decades to remotely acquire information about targets of interest such as their range and relative velocity. Various transmit modes and waveforms have been developed to increase radar effectiveness in specific situations, but each method has its limitations. Some obstacles that frequently prevent target detection regardless of radar parameters are the presence of both internal and external noise and backscatter from objects other than the target of interest. Efforts have been made in recent years to overcome these challenges by implementing various noise reduction and clutter suppression techniques [1].

The radar system used throughout this project is referred to as a dual-purpose radar because it is intended to find the range of stationary targets while simultaneously determining the range and velocity of moving targets in the midst of static clutter. These two purposes will be achieved by implementing stretch processing while operating in FMCW mode at a center frequency of 108 GHz.

FMCW mode was preferred over other transmit modes because it allows for the implementation of stretch processing and because of the benefits it provides when dealing with close-range targets. For instance, blind-range and eclipsing—both of which put limitations on pulse duration—need to be considered for pulse and chirp radar systems, but they are not significant factors for FMCW radar. The decision to operate in W-Band (75 – 110 GHz) is more for practical reasons. Specifically, transmitting mm-wavelength signals allows for relatively small transmit and receive antennas to be used, making the radar system more suitable for a larger range of applications.

Similar dual-purpose radar systems have been developed for use in the automotive and aerospace fields, and some of these use waveforms and methods similar to those proposed in this thesis [2]–[4]. However, two aspects of this radar system that set it apart from most others are the frequency offset introduced between the transmit signal and reference signal—which makes it easier to distinguish positive and negative Doppler—and the method of clutter suppression that this frequency offset enables.

The proposed clutter suppression method suppresses return signals from all static targets (after range information has been obtained) so that moving targets can be detected more easily. This requires that the transmitted signal be a triangular waveform with equal upchirp and downchirp durations. When this is the case, the received echo signals can be separated into two complementary data sets, an upchirp data set and a downchirp data set. Static clutter in the downchirp data set will always yield positive beat frequencies, while static target beat frequencies in the upchirp data set will be mirrored across the frequency offset (or across DC if no offset exists). By manipulating chirp duration, it can be ensured that moving target beat frequencies will either be positive in both data sets, or negative in both data sets. This means that one data set will contain signal data in which the moving target signal is spectrally isolated (separated in frequency) from the static clutter in that data set. Because the clutter signals from this first data set will be mirror images of the clutter signals from the second data set, they can then be used to suppress the clutter in the second data set, greatly improving moving target detection in that data set. Once the moving target signals are recovered from each data set, they can then be used to solve for moving target range and radial velocity simultaneously and unambiguously.

Chapter 2. System Design and Signal Progression

This radar system is comprised of two channels as shown in the diagram in figure 2-1 below. The Tx-channel supplies the transmit antenna with a 600 MHz bandwidth triangular waveform centered at 108.48 GHz. The Rx-channel provides a reference signal to the receive antenna, which is nearly identical to the signal produced in the Tx-channel, but with a +3 MHz offset. The reason for the offset is discussed at the end of this chapter.

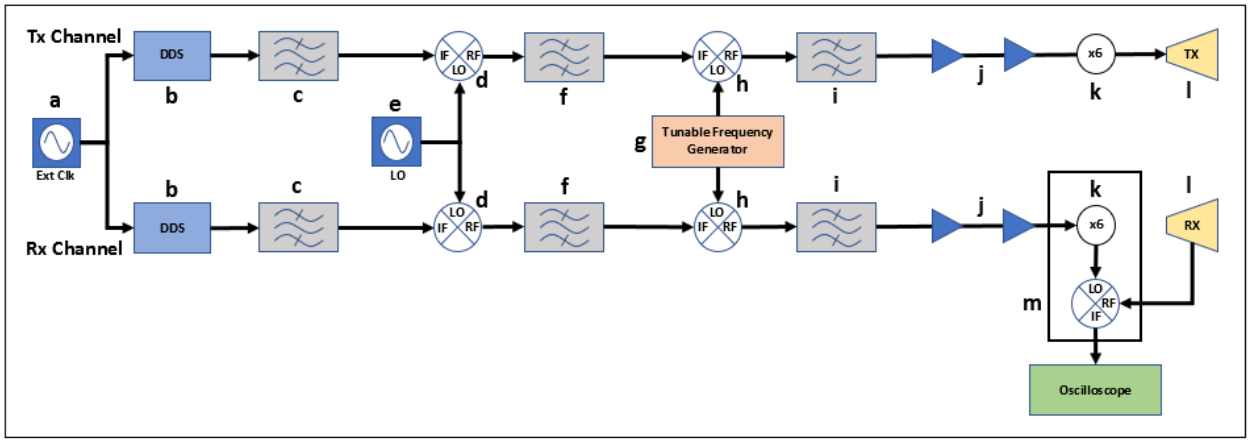

Figure 2-1: Component level block diagram of Radar System

A similar diagram containing the signal power at the output of each component is provided in Appendix B. Additionally, select component manufacturer datasheets can be found in Appendix C. Names and descriptions of the various components are listed in table 2-1 below.

Table 2-1: System block diagram component descriptions.

Symbol	Name	Description
a	Signal Generator	N9310A 9kHz-3.0GHz RF Signal Generator from Agilent
b	Digital Synthesizer	AD9915 Direct Digital Synthesizer (DDS) from Analog Devices
c	Bandpass Filter	ZFBP-2400-S+ 2300-2500MHz bandpass filter from Minicircuits
d	Mixer	ADRF6780 wideband RF mixer from Analog Devices
e	Signal Generator	68147B 10MHz-20GHz Synthesized Sweep Generator from Wiltron
f	Bandpass Filter	ZVBP-8250-S+ 8025-8475MHz bandpass filter from Minicircuits
g	Signal Generator	68247B 10MHz-20GHz Synthesized Signal Generator from Anritsu
h	Mixer	M2B-0226 triple-balanced mixer from Marki Microwave
i	Bandpass Filter	FB-1500 12-18GHz bandpass filter from Marki Microwave
j	Amplifier	Zx60-183A-S+ 6-18GHz Wideband Amplifier from Minicircuits
k	X6 Multiplier	WR10AMC-I amplifier/multiplier chain from Virginia Diodes
l	Antenna	WR-10 75-110GHz Conical Horn Antenna from Virginia Diodes
m	X6 Mult/Mix Assy.	WR10MixAMC-I mixer/amp/multiplier chain from Virginia Diodes

The first component **(a)** in the block diagram in figure 2-1 is a signal generator which serves as a 2 GHz external clock for the Direct Digital Synthesizer (DDS) in each channel. Feeding both DDSs with a single clock helps to ensure that both channels stay synchronized while the system is in operation.

Focusing now on the Tx-channel, the next component in the radar system is the DDS **(b)**. This DDS has been programmed to output a triangular waveform centered at 430 MHz with a

bandwidth of 100 MHz. The waveform consists of an upchirp with a start frequency of 380 MHz and stop frequency of 480 MHz, followed immediately by a downchirp with a start frequency of 480 MHz and a stop frequency of 380 MHz. The DDS produces the upchirp portion of the triangular waveform by making a finite number of small incremental steps (32768) over the course of 0.5 milliseconds. Each step is approximately 3.05 kHz, but these frequency jumps are relatively small compared to the total 100 MHz bandwidth, and are made in such short amounts of time that the result is a good approximation of an analog chirp. The downchirp is produced in a similar manner, also over 0.5 milliseconds, making the total waveform duration 1 ms long. But since this radar system operates in Continuous Wave (CW) mode, the triangular waveform just described is transmitted continuously during operation.

Because the DDS is fed with an external clock frequency (f_{clk}) of 2 GHz, the DDS output consists of the initial 430 MHz signal and images at integer multiples of 2.0 GHz (± 430 MHz) such that a frequency component exists in each subsequent Nyquist zone as seen in figure 2-2.

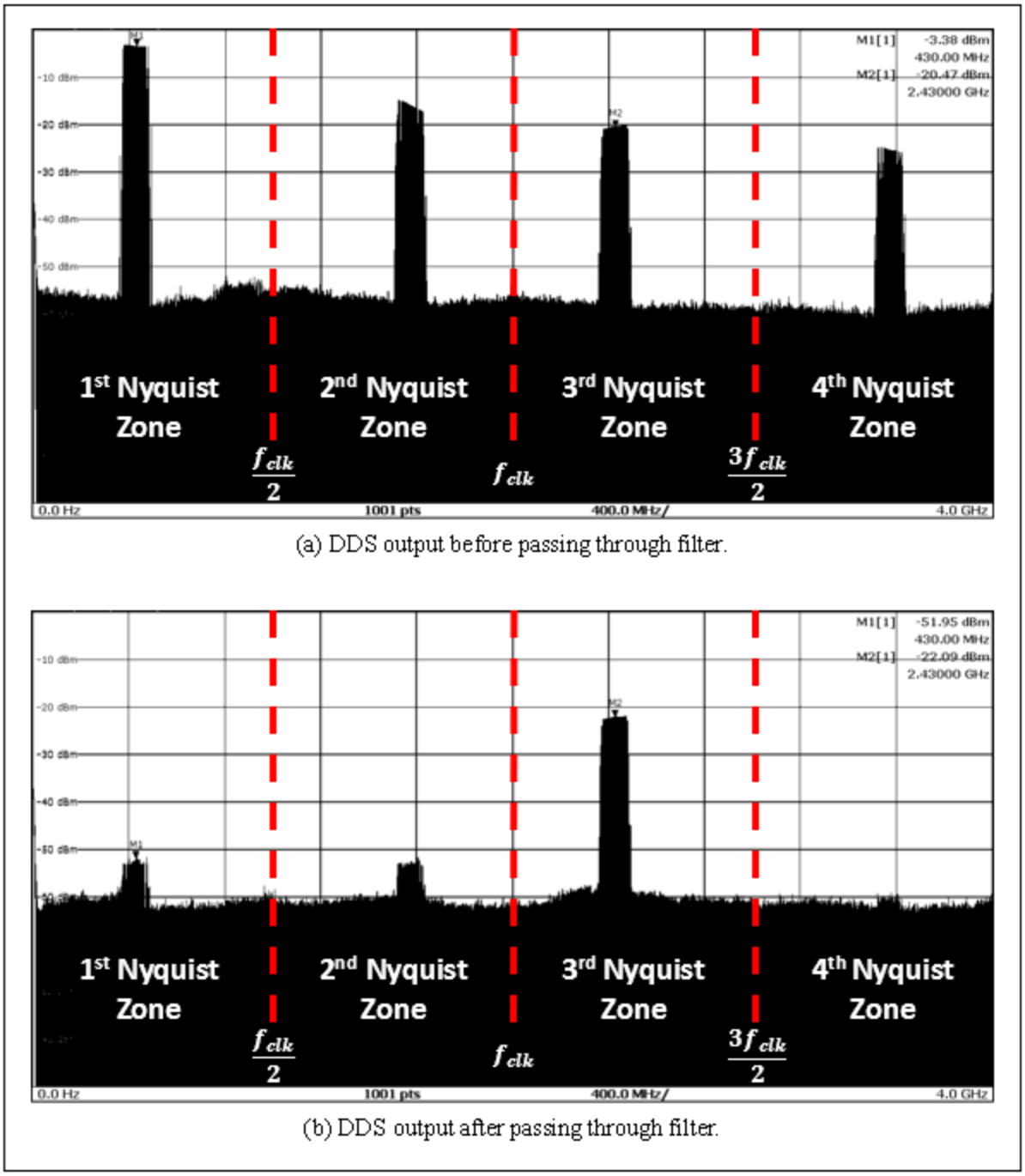

Figure 2-2: Spectrum analyzer shows the 430 MHz signal (indicated by marker M1) and it's subsequent images produced in each Nyquist Zone. Plot (a) contains the unfiltered DDS output. Plot (b) shows the filtered DDS output leaving only the desired image centered at 2.43 GHz (indicated by marker M2). This signal lies in the 3rd Nyquist zone, between the 2 GHz DDS clock frequency (f_{clk}) and $3f_{clk}/2$.

To remove any unwanted signal components, it was necessary to place a bandpass filter **(c)** at the output of the DDS. A filter was selected such that the passband allowed only the signal image in the 3rd Nyquist zone to pass through, while greatly attenuating the other images. The resulting frequency spectrum, with the strongest signal centered at 2.43 GHz, is seen in figure 2-2b.

It was advantageous to work with the signal image lying in the 3rd Nyquist Zone because that image is separated from DC by an additional 2 GHz over the 430 MHz baseband signal. The reason that separation is important is because the next stage in the radar system **(d)** upconverts the signal by mixing it with a 6.0 GHz carrier frequency produced in a separate signal generator **(e)**. Mixers are typically susceptible to some amount of LO leakage, meaning that along with the desired RF signal output that comes as a result of mixing the IF signal with 6.0 GHz, there will also be a 6.0 GHz signal at the output of the mixer which can be difficult to filter out if it is too close in frequency to the desired signal. But with the added separation from DC that comes from selecting the 3rd Nyquist Zone image, when it is upconverted by the 6.0 GHz carrier frequency, the signal of interest will appear at 8.43 GHz instead of 6.43 GHz. The increased separation between the desired signal and the LO leakage makes it significantly easier to filter out the 6.0 GHz leakage signal, as can be seen in figure 2-3 below.

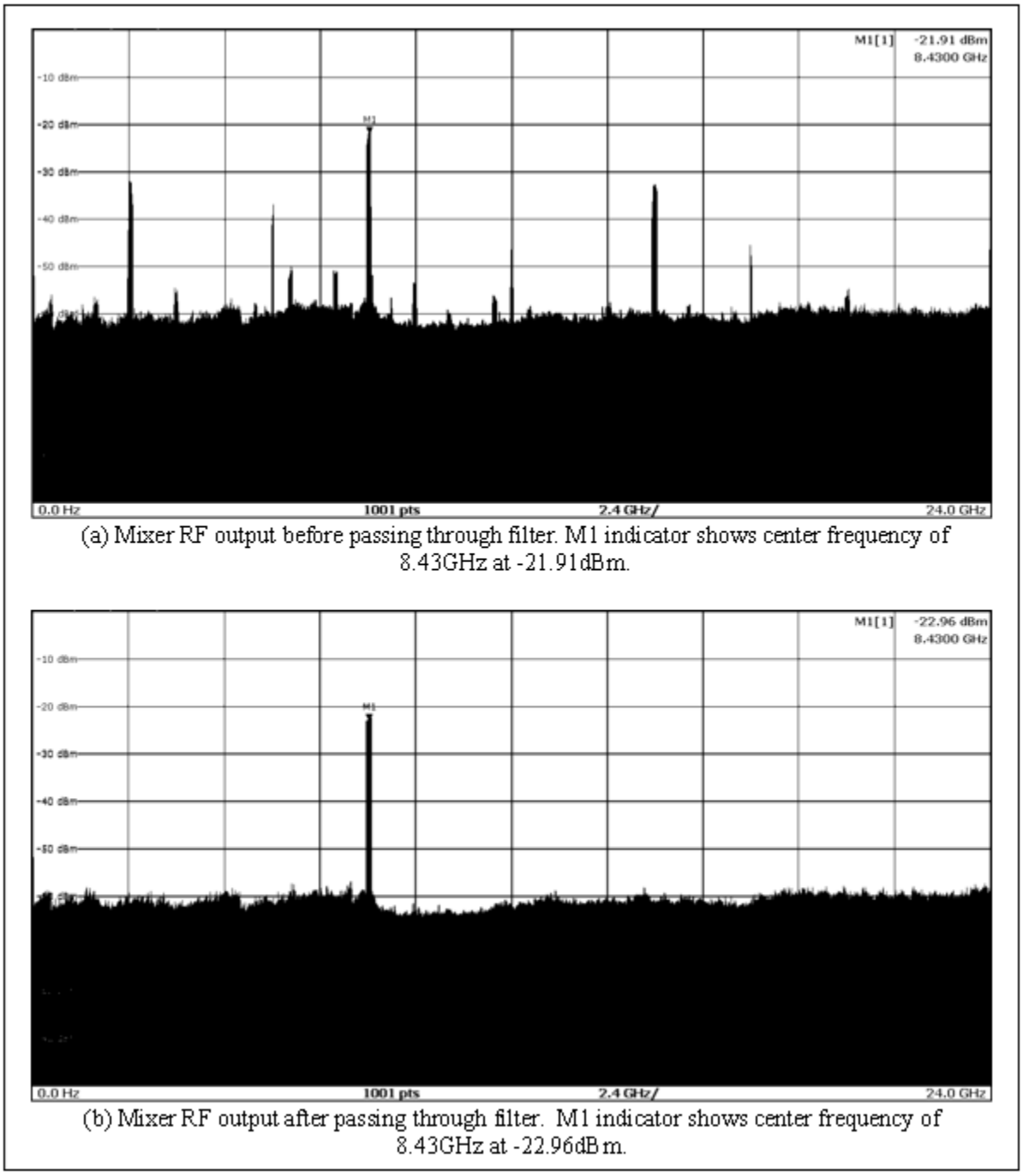

Figure 2-3:Spectrum analyzer shows the ADRF6780 mixer output before and after passing through filter.

After the 8.43 GHz RF signal passes through the bandpass filter, it is upconverted via another mixer **(h)**, this time with a 9.65 GHz carrier frequency produced by a tunable frequency generator **(g)**. The reason a tunable frequency generator was used for the LO input into the

second mixer **(h)** was because it added flexibility into the overall system design by increasing the radar operating range to include all W-Band frequencies (75-110 GHz).

Although the system can operate at any W-Band frequency, through trial and error, with the current filters and amplifiers in place, it was determined that the system performed best with the tunable frequency generator set to 9.65 GHz, which resulted in a mixer RF output center frequency of 18.08 GHz (see figure 2-4).

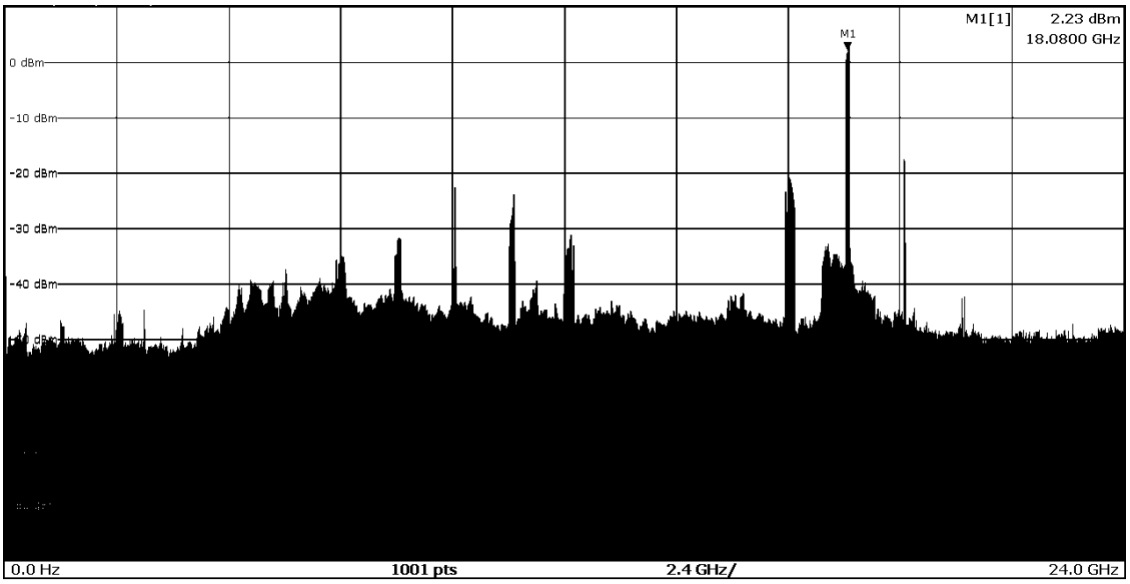

Figure 2-4: Spectrum analyzer shows final 18.08 GHz signal before passing through the WR10AMC-I x6 multiplier.

This signal passes through a final bandpass filter **(i)** before being amplified **(j)** to levels appropriate for the x6 multiplier chain **(k)**, which jumps the signal center frequency up to 108.48 GHz. Another effect of the x6 multiplier is that the total bandwidth of the signal is also increased by a factor of 6. Now, instead of having a 100 MHz bandwidth, the resulting signal is transmitted with a bandwidth of 600 MHz, which will improve spatial resolution and impact beat frequency, as will be discussed shortly.

As previously stated, the Rx-channel produces a signal identical to the Tx-channel, but with a 3 MHz offset. The only other notable difference between the two channels is that the x6 multiplier chain in the Rx-channel also includes a mixer **(m)**. This is so that once the transmitted signal is received by the Rx-channel antenna **(l)**, the resulting signal can be compared to (mixed with) the reference signal produced by the Rx-channel, and the difference between the two signals can be analyzed to yield information about target range and velocity.

The final component in the system diagram is a Keysight DSO-X 3024A oscilloscope which was used for collecting and recording signal data. Because final signal data will lie in the region of 2.9 MHz to 3.1 MHz, the oscilloscope needed to have a sampling rate of at least 6.2 MHz to satisfy Nyquist sampling theory. For this oscilloscope, the sampling rate is limited by various factors including the number of active input channels while recording and the amount of time that is being recorded. Certain tests were performed using two active input channels and sampling for up to 150 ms, which limited the sampling rate to 10 MSPS. Other tests also required two active input channels but only 100 ms of recording time, allowing for a sampling rate of 20 MSPS. Therefore, all tests performed allowed for a sampling frequency high enough to satisfy the Nyquist sampling rate.

Chapter 3. Stretch Processing

Beat Frequency

The method used here to determine target range and velocity is known as Stretch Processing and results in what is referred to as a Beat Frequency (f_b). The term "beat frequency" gets its name from the acoustic phenomenon which takes place when two audible tones of different frequencies are played simultaneously. When this occurs, the sound waves add constructively and destructively to produce a third tone with a frequency equivalent to the difference between the two original tones. If the two original tones are close enough in frequency, a periodic beat can be heard [5].

A similar effect can be achieved in electromagnetics when two signals of different frequencies are multiplied together using a mixer. The product of the signals consists of numerous terms, the dominant of which are a sum and a difference term. The sum term is merely a signal which has a frequency equal to the sum of the two original frequencies, while the difference term is equivalent to their difference. The benefit of taking the difference between two signals is that data contained in a high frequency signal—which can be difficult to process—can be brought down to a much lower and more manageable frequency if it is 'mixed' with another signal of a slightly different frequency. For instance, if the signal of interest were 12.2 GHz, and this were mixed with a 12.0 GHz signal, the dominant resulting terms would be one signal at 24.2 GHz and another signal at 0.2 GHz (200 MHz). The difference term in this example is not specifically a 'beat frequency', but these steps are applied directly in the process of obtaining the beat frequency.

Beat frequency is, essentially, the instantaneous difference in frequency between a transmitted signal and the reference signal. In a radar system, once a known signal is transmitted, the most important thing about the return signal is how it varies from what was transmitted. This difference is what gives information about the range and radial velocity of a target, based on the round-trip travel time and any Doppler shift in the return signal. If a signal is received simultaneously using two or more receivers, the difference between each of the received signals will yield additional information about the angle of elevation and azimuth to the target, as well as the direction the target is moving.

With one transmitting antenna, a separate co-located receiving antenna, and a stationary target, the method for finding the target beat frequency is illustrated in figure 3-1. Once beat frequency is known, determining the range of a stationary target is trivial.

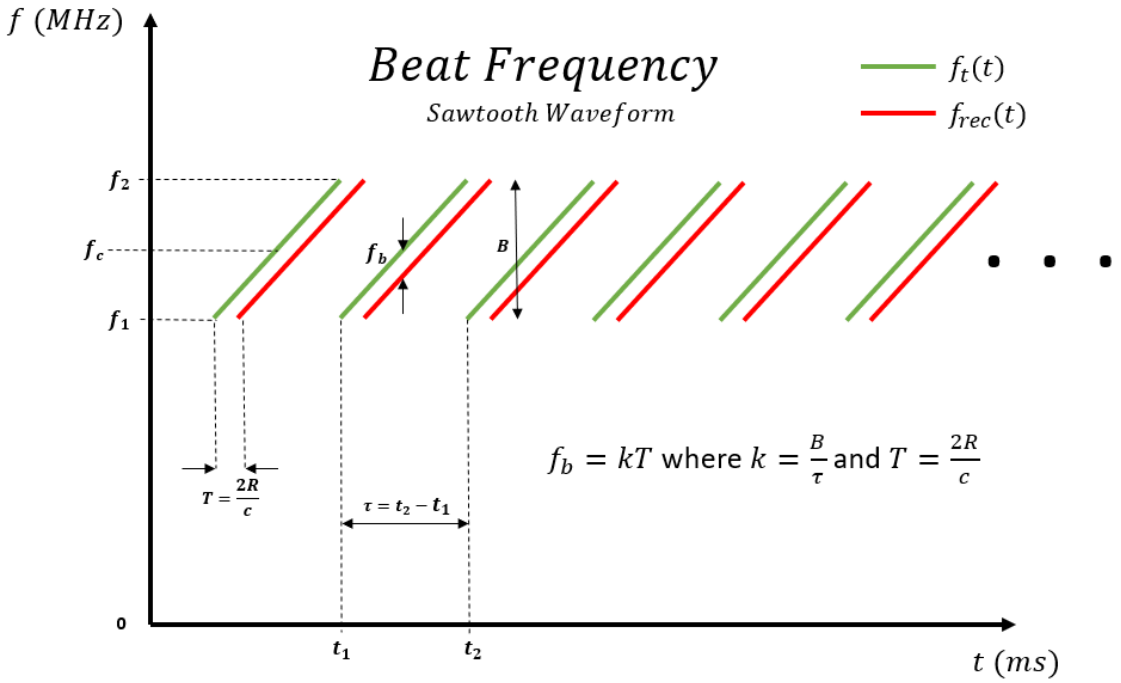

Figure 3-1: Plot depicting the difference in a transmitted FMCW signal and corresponding return signal as a function of time, and how to use their relationship to obtain a beat frequency (Transmitted signal is in green, received signal is in red).

The green trace in the plot above represents a transmitted signal whose frequency increases from an initial frequency (f_1) to a set upper frequency (f_2) over a predetermined amount of time. This type of linear frequency modulation is known as an upchirp, and it is repeated continuously in an FMCW system. The slope of the line (k) is determined by both the chirp duration (τ), and the bandwidth (B) of the transmitted signal. The red trace in the figure represents the return signal that would be obtained if the transmitted signal had scattered off a stationary point target at some distance (R) before being picked up by a radar receiver that is co-located with the transmitter. The round-trip travel time (T) is equal to the time it would take for a signal moving at the speed of light (c) to travel to and from the target. This difference in time is shown as the horizontal separation between each transmitted chirp (in green) and the subsequent return signal (in red).

By taking the difference in frequency between the two traces at any given point in time, the beat frequency (f_b) can be obtained. In practice, this is done by mixing a copy of the transmitted signal with the time-delayed return signal and looking at the difference, as shown in figure 3-2 below.

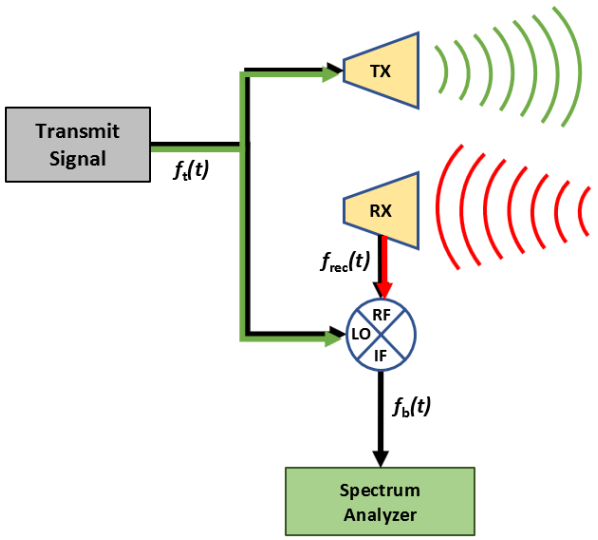

Figure 3-2: A copy of the transmit signal $f_t(t)$ is sent to the mixer LO port and is mixed with the received signal $f_{rec}(t)$ at the mixer RF port, resulting in a downconverted IF signal where the target beat frequency $f_b(t)$ can be determined.

Once the beat frequency has been obtained, assuming the target is stationary, the range (R) to the target can easily be derived by rearranging the beat frequency equation as follows:

$$f_b = kT = \frac{2BR}{\tau c} \tag{3.1}$$

$$R = \frac{f_b \tau c}{2B} \tag{3.2}$$

At this point, all values on the right side of equation (3.2) are known. Beat frequency (f_b) is known because it is measured at the IF output of the final mixer. Chirp duration (τ) and bandwidth (B) are also known because they are set system parameters. And the speed of light (c), for the purposes of this project, can be approximated as $3\text{x}10^8$ m/s.

However, if the target does have some non-zero velocity with respect to the radar system, the target return signal will have an additional frequency shift based on its Doppler frequency

(f_D), which is proportional to the velocity (v) of the target and the operating frequency (f_c). Doppler frequency can be determined as:

$$f_D = -\frac{2v}{\lambda} = -\frac{2vf_c}{c} \tag{3.3}$$

where velocity is defined to have a negative value for targets moving towards the radar system, and a positive value for targets moving away from the radar system.

In the case that the target is moving, the equation for obtaining the beat frequency takes on a second term to account for the added Doppler frequency. Therefore, equation (3.1) can be rewritten to describe the beat frequency of a moving target as:

$$f_b = f_{bR} + f_D = \frac{2BR}{\tau c} - \frac{2vf_c}{c} \tag{3.4}$$

where f_{bR} is the beat frequency due to range and is equivalent to f_b in equation (3.1).

The addition of the second term includes two more variables, velocity (v) and center frequency (f_c). Just like the other system parameters, center frequency is also known. Therefore, the only unknown variables are range and velocity, which are dependent on the target. These remaining two variables are coupled together in the sense that neither range nor velocity can be determined without some prior knowledge of the other. If the target's range is known to be constant, the second term drops out, and target range can be identified. But if the target is moving at some unknown velocity, there will be no way to determine what portion of the measured beat frequency is due to target range, and what portion is due to its velocity. Therefore, using the method described above, range and velocity cannot be unambiguously determined.

This problem was overcome by transmitting a triangular waveform instead of a sawtooth waveform. A triangular waveform is comprised of alternating upchirps and downchirps. This waveform is preferable because the return signal received during an upchirp is different than the signal received during a downchirp. Now, despite the target having essentially the same range and velocity from one upchirp to the subsequent downchirp, the calculated beat frequency will be different. See figure 3-3 below.

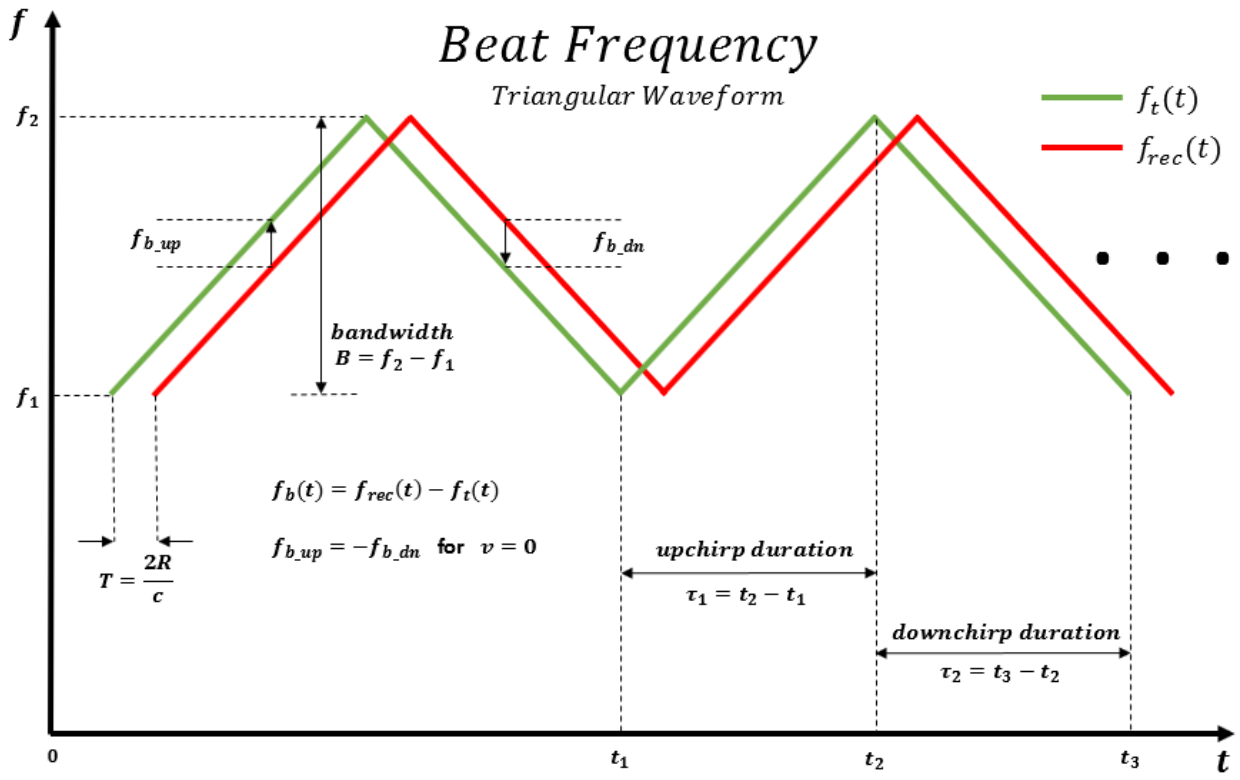

Figure 3-3: A triangular waveform yields two different beat frequencies (f_{b_up} & f_{b_dn}) for the upchirp and downchirp portions of the waveform. Both beat frequencies are accurate and can be used together to determine the range and velocity of a target. If a target is stationary, the Doppler component of the beat frequency is equal to 0, therefore $f_{b\_up} = -f_{b\_dn}$.

The upchirps and downchirps in the triangular waveform depicted in figure 3-3 have the same chirp duration and absolute bandwidth. However, with beat frequency ($f_b(t)$) defined as the received signal ($f_{rec}(t)$) minus the transmit signal ($f_t(t)$), the range component of beat frequency (f_{bR}) takes on a negative value during the upchirp portion of the waveform. This means that the recovered beat frequency will alternate between two different values (f_{b_up} & f_{b_dn}) according to equations (3.5) and (3.6) below.

$$f_{b\_up} = -\frac{B2R}{\tau_1 c} - \frac{2vf_c}{c} \tag{3.5}$$

$$f_{b\_dn} = \frac{B2R}{\tau_2 c} - \frac{2vf_c}{c} \tag{3.6}$$

Having two different beat frequencies for a single target is beneficial because now there are two equations which can be used to solve for the two unknown variables, range and velocity. Note that having the chirp durations (τ_1 & τ_2) set to equal lengths is not necessary to determine range and velocity, but doing so simplifies static clutter suppression.

3 MHz Offset

When performing Stretch Processing, it is typical to use a copy of the transmit signal as a reference with which to compare the target echo signal at the receiver, as shown in figure 3-2. However, it became necessary to introduce a frequency offset between the transmit signal and reference signal for two reasons.

First, if the transmit signal $f_t(t)$ and reference signal $f_{ref}(t)$ are the same, then the relationship $f_{b\_up} = -f_{b\_dn}$, as stated earlier, still holds for stationary targets. But when this is

true, it is difficult to determine which data was the result of an upchirp and which was from a downchirp. To illustrate this point, consider the following scenario where a triangular waveform is used to detect point targets set at ranges R1, R2, R3 & R4. The resulting spectrum would resemble figure 3-4a below, with the beat frequencies for each target collected during upchirps appearing as negative frequencies, and the target beat frequencies collected during downchirps appearing as positive frequencies.

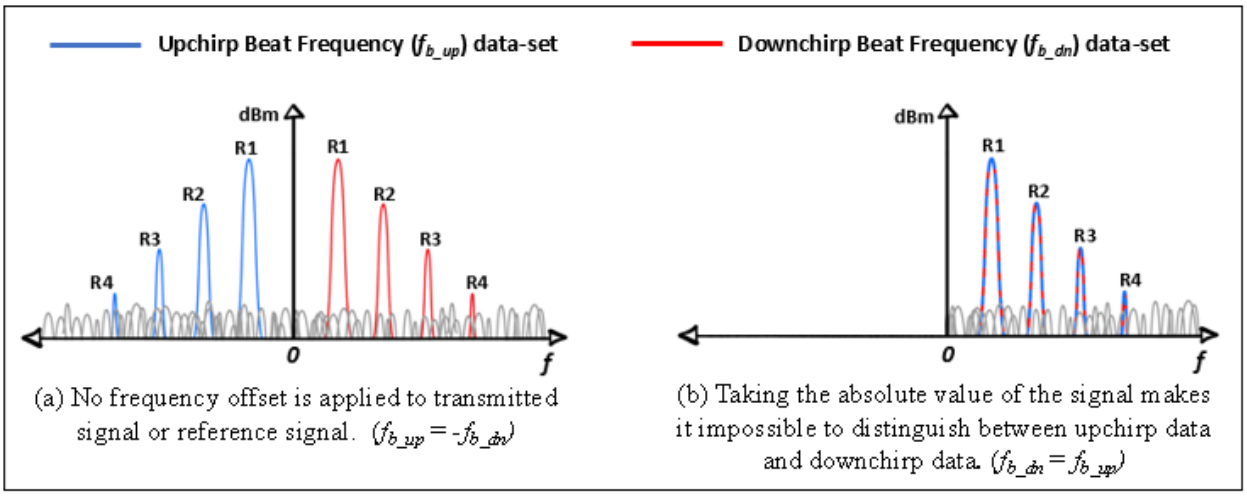

Figure 3-4: Targets are detected at ranges R1, R2, R3 & R4 using a triangular waveform with no frequency offset between the transmit signal and reference signal. Stationary target beat frequencies overlap once they are aliased across DC.

As seen in figure 3-4b, the negative beat frequencies are aliased over the 0Hz axis and perfectly overlap the positive beat frequencies, making f_{b_up} and f_{b_dn} indistinguishable. This is adequate when viewing objects that are known to be stationary—range can still be determined without consequence—but when viewing moving objects, it is important to be able to determine which data set is comprised of upchirps and which is comprised of downchirps, as will be shown in a later section.

The second reason for implementing a frequency offset was because receiver module interference was observed at approximately 120 kHz, with subsequent harmonics appearing up to 2.5 MHz (see figure 3-5). The source of the interference could not be eliminated, so placing a filter at the receiver output was considered. However, it was determined that the signals could not be filtered without also filtering the target beat frequencies, which were expected to appear in the 100 kHz region based on predetermined chirp duration and signal bandwidth parameters.

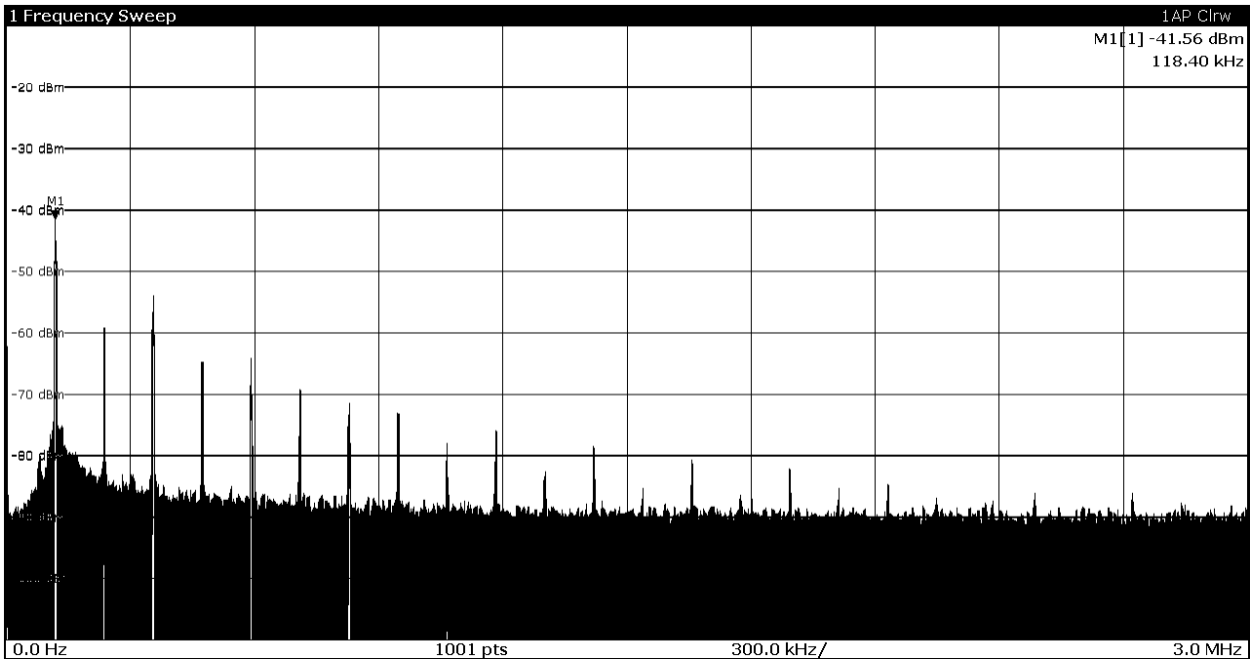

Figure 3-5: Unwanted signals generated within the WR10MixAMC receiver mixer/multiplier/amplifier chain.

To avoid the problem area, a frequency offset of 3 MHz was applied to the transmit signal. It is important to note how adding the 3 MHz frequency offset to either the transmit signal or the reference signal affects the final system output. Let the offset Δf_c be defined as the difference between the center frequency of the transmitted signal (f_{t_c}) and the center frequency of the reference signal (f_{ref_c}).

$$\Delta f_c = \left(f_{t\_c} - f_{ref\_c}\right) \tag{3.7}$$

The beat frequency must also be redefined to account for an added frequency offset. Therefore, equations (3.5) and (3.6) become:

$$f_{b\_up} = -\frac{2BR}{\tau c} - \frac{2vf_c}{c} + \Delta f_c \tag{3.8}$$

$$f_{b\_dn} = \frac{2BR}{\tau c} - \frac{2vf_c}{c} + \Delta f_c \tag{3.9}$$

Now, for the case that a +3 MHz offset is applied to the transmit signal, it follows that,

$$\Delta f_c = \left(f_{t\_c} + 3\ MHz\right) - f_{ref\_c} = 3\ MHz \tag{3.10}$$

such that f_{b_up} and f_{b_dn} will simply be shifted to the right by 3 MHz. And since the target return signals from the downchirp data set initially had positive values while the target return signals for the upchirp data set had negative frequency values, once they are offset by +3 MHz, the upchirp beat frequencies will appear below 3 MHz, and the downchirp beat frequencies will appear above 3 MHz, as seen in figure 3-6a.

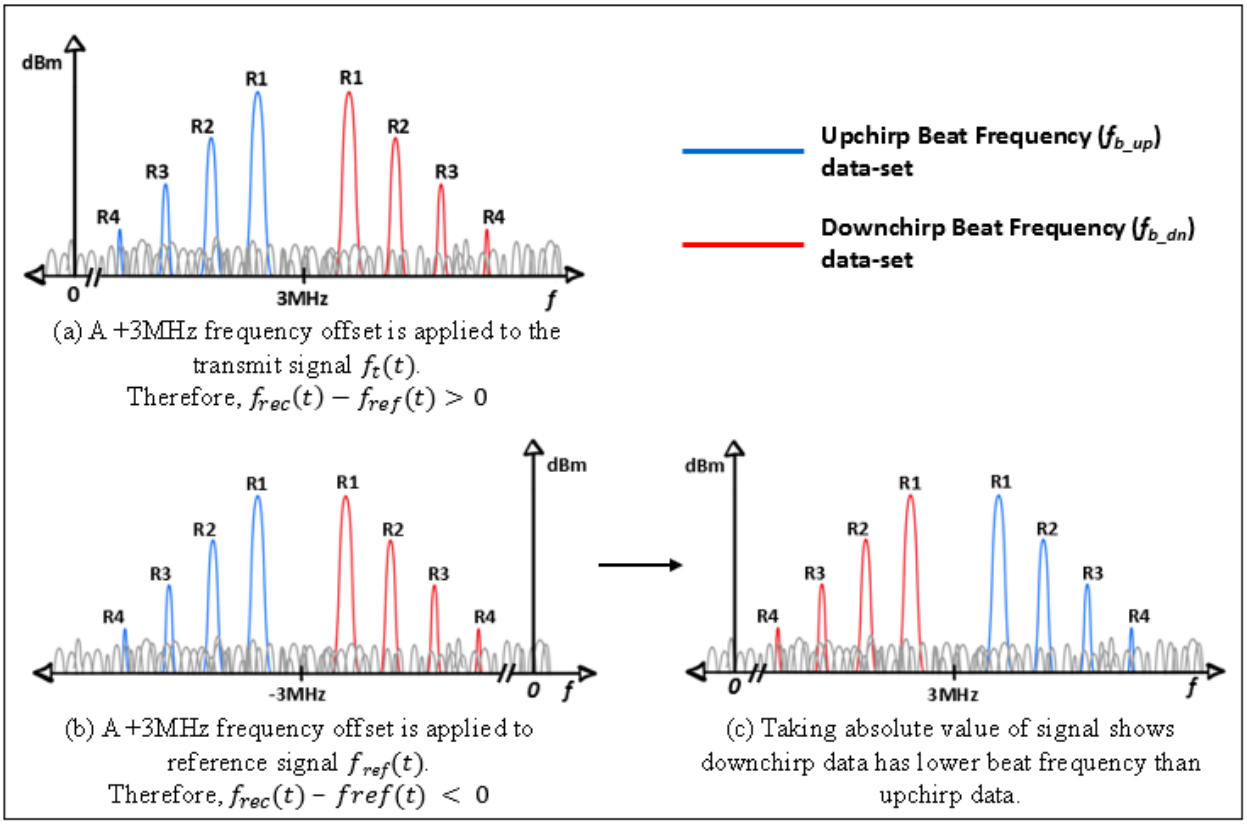

Figure 3-6: Illustration of what the spectrum might look like if targets were detected at ranges R1, R2, R3 & R4 using a triangular waveform with a 3 MHz offset between the transmit signal and reference signal. Applying the +3 MHz offset to the reference signal (a) has an effect opposite to if it were applied to the transmit signal (b and c).

If, instead, a +3 MHz offset were applied to the reference signal, it is apparent that Δf_c would be negative as seen here,

$$\Delta f_c = f_{t\_c} - \left(f_{ref\_c} + 3\ MHz\right) = -3\ MHz \tag{3.11}$$

and both f_{b_up} and f_{b_dn} would be shifted to the left by 3 MHz (see figure 3-6b). Once again, because negative frequency is not very physically meaningful, it is necessary to take the absolute value of the signal spectrum. However, by doing so we see in figure 3-6c that the target beat frequencies corresponding with the downchirp data set are now less than 3 MHz, while the target beat frequencies from the upchirp data set are greater than 3 MHz. Thus, applying the +3 MHz

offset to the reference signal yields results opposite to what was seen when the transmit signal was offset by +3 MHz.

Regardless of which channel is offset, the resulting signal is sufficient to determine target range and velocity because, in both cases, the upchirp data set and downchirp data set are distinguishable. This means that the decision of which channel has a frequency offset is arbitrary, but it must still be known and accounted for to determine which data was collected during an upchirp and which was collected during a downchirp. Unless otherwise stated, all tests and experiments discussed in this paper were done with a +3 MHz offset applied to the transmit signal $f_t(t)$, such that the resulting data and plots that are shown herein are most closely represented by the depiction shown in figure 3-6a.

Chapter 4. Test Setup & Results

Test Procedure & Data Processing

A series of tests were conducted to calibrate the radar system and ensure that both range and velocity detection capabilities were functioning properly. The radar system was programmed to continuously transmit a triangular waveform (0.5 ms upchirp & 0.5 ms downchirp) with 600 MHz bandwidth, centered at 108.48 GHz. Return signal data was collected by mixing the target echo signal (offset by +3 MHz) with the reference signal and routing the mixer output to an oscilloscope where it was then recorded at a sampling rate of 20 MSPS.

While the triangular waveform is being output by the DDSs, each DDS also sends a trigger signal to the oscilloscope. The trigger signal is comprised of a series of impulses, each of which mark the beginning of an upchirp or downchirp. The trigger signal and the downconverted received signal are recorded simultaneously by the oscilloscope so that each sample of received signal data can be properly characterized as to whether it occurred during an upchirp or a downchirp. Knowing when each upchirp and downchirp begins is especially important because it dictates the beginning and end of the data segments on which fast-time FFTs are performed. After the signal data is recorded by the oscilloscope, they are then saved in binary format and post-processed using MATLAB. A plot of 100 ms of recorded signal data overlaid with the DDS trigger signal is shown in figure 4-1 below.

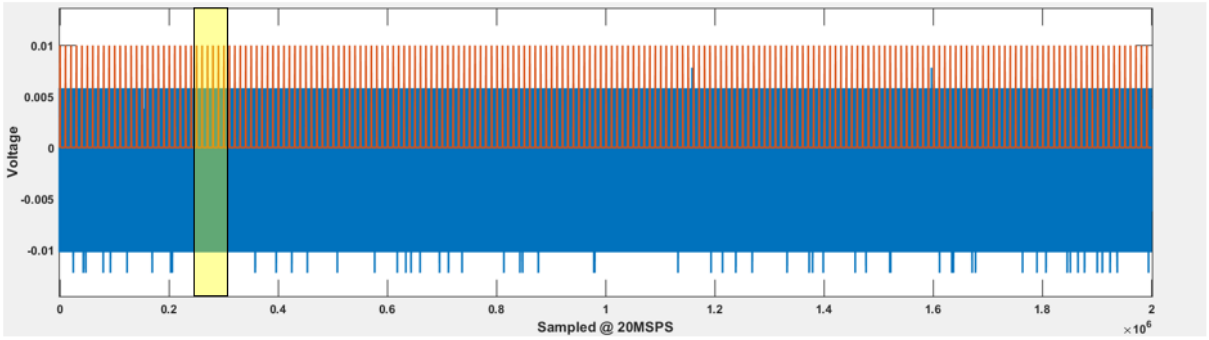

(a) Raw signal data (in blue) overlaid with the DDS trigger (in red). Both are recorded for 100 ms at a sampling rate of 20 MSPS. The yellow-highlighted portion is approximately 2.5 ms of data, and is seen close-up in figure (b).

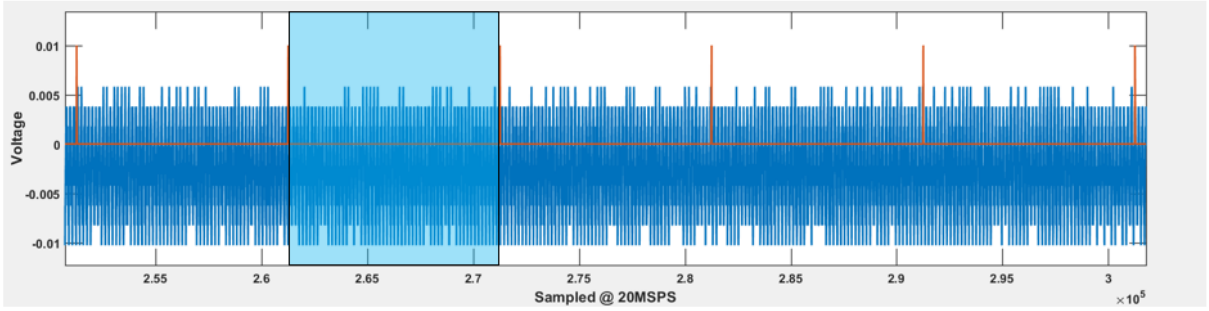

(b) The blue-highlighted portion here represents a single 0.5 ms upchirp or downchirp. Because the upchirp duration and downchirp duration are equivalent, each section cannot be classified until additional processing takes place.

Figure 4-1: Unprocessed signal data overlaid with the DDS trigger signal.

As seen in figure 4-1, based on the raw signal data and DDS trigger alone, it is impossible to determine whether each 0.5 ms segment corresponds to an upchirp or a downchirp. However, by performing FFTs on the first two segments and analyzing the frequency content around 3 MHz, the upchirp/downchirp classification can be determined for the whole 100 ms data set. This is done by first verifying that the target being observed is stationary. A stationary target will always satisfy the condition that the measured beat frequency from one segment will have the same absolute value as the beat frequency measured during an adjacent segment (i.e. $f_{b\_up} = -f_{b\_dn}$). Once stationarity is confirmed, the segment that corresponds to an upchirp

will be the segment that yields a negative beat frequency. It then follows that every *other* subsequent segment will also correspond to an upchirp. The whole data set can then be parsed into two separate sets of data, as seen in figure 4-2. The set that is comprised of data received during upchirps will be referred to hereafter as an upchirp data set, and data collected during downchirps will be referred to as a downchirp data set.

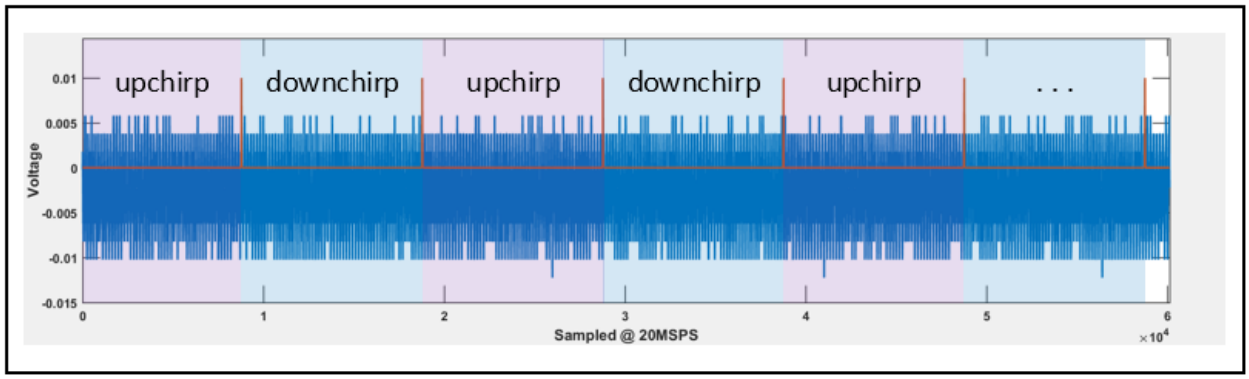

Figure 4-2: Received signal data separated into upchirp and downchirp data sets.

Static Target Range Finding and Radar Calibration

To verify that target range was being detected accurately, the radar system was placed at one end of a room while a 3.2-inch trihedral (RCS ~ 7.7 dBsm) and a 6-inch trihedral (RCS ~ 18.7 dBsm) were positioned at varying known distances in front of the radar antennas, as seen in figure 4-3. By evaluating the range equation for stationary targets, target range can be determined once beat frequency is measured. Rearranging equations (3.5) and (3.6) and setting velocity equal to zero gives the following relationship between target range (R) and upchirp and downchirp beat frequencies.

$$R = -\frac{f_{b\_up}\tau_{up}c}{2B} = \frac{f_{b\_dn}\tau_{dn}c}{2B} \tag{4.1}$$

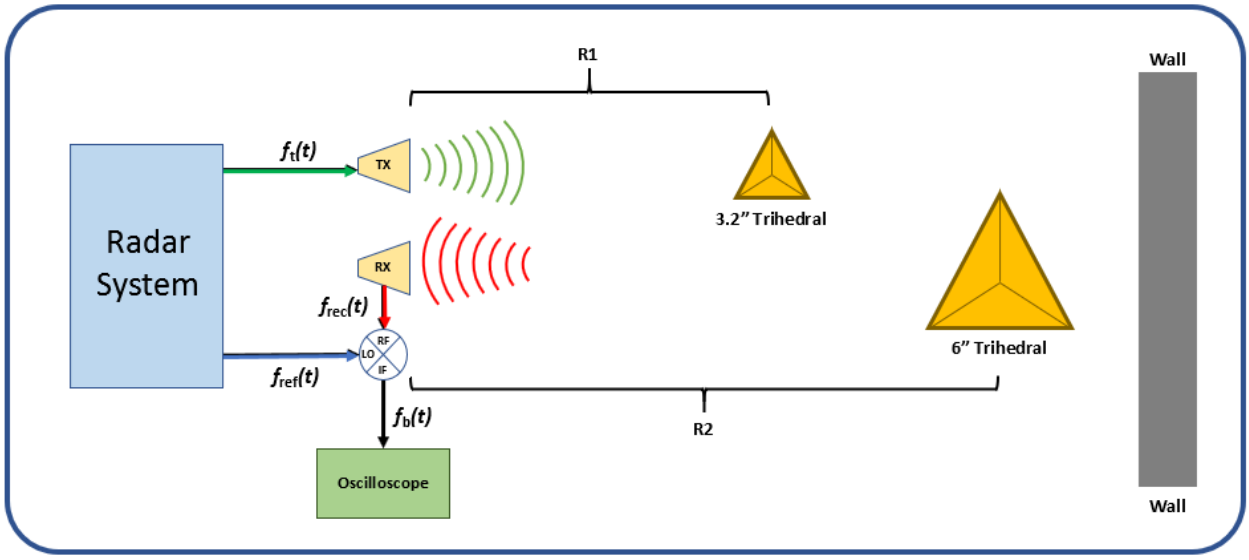

Figure 4-3: Stationary target range detection test setup for two trihedrals placed at ranges R1 and R2.

For this test, the 3.2-inch trihedral was placed at a range (R1) of 4.75 meters, and the 6-inch trihedral was placed at a range (R2) of 6.45 meters. If these ranges are plugged into equation (3.4), along with transmit signal bandwidth (600 MHz) and chirp duration (0.5 ms), the expected beat frequencies for the trihedrals at R1 & R2 are approximately $\pm 38.0\ kHz$ & $\pm 51.6\ kHz$, respectively. However, accounting for the 3 MHz offset between the received signal $f_{rec}(t)$ and the reference signal $f_{ref}(t)$, the expected target beat frequencies become $3\ MHz \pm 38.0\ kHz$ for the 4.75 m target, and $3\ MHz \pm 51.6\ kHz$ for the 6.45 m target. Since the 3 MHz offset exists in all data collected for this project, it can simply be subtracted from the measured beat frequency to determine the actual beat frequency due to target range and velocity. Figure 4-4 shows the resulting signal data with the 4.75 m and 6.45 m targets in place.

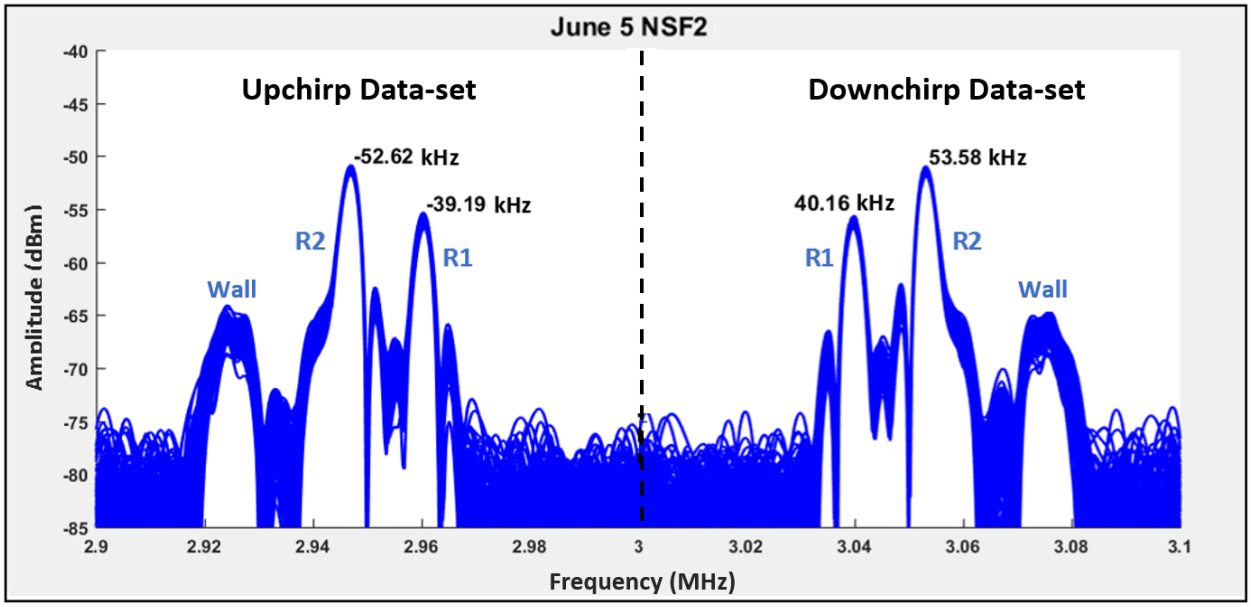

Figure 4-4: Target beat frequencies from the upchirp and downchirp data sets are approximately symmetric about the 3 MHz offset, confirming that these are stationary targets. Any differences between target beat frequencies in the two data sets are most likely because the radar system is not calibrated. The figure heading indicates that no shot was fired (NSF) during this test.

In figure 4-4, an upchirp data set and a downchirp data set are shown. Each data set contains two distinct peaks (labelled R1 and R2) and their associated beat frequencies after the 3 MHz offset has been subtracted out. The pair of beat frequencies labelled R1 both belong to the same target, despite having slight differences. The pair of beat frequencies belonging to the target at R2 are similarly different. This should not be the case for stationary targets. Taking the average of the individual pairs of beat frequencies for each point target reveals that they are actually centered around 3.00048 MHz. This additional 0.48 kHz offset could be due to the effects of fluctuating temperature on various radar components, or it could be a result of finite word-length rounding errors within the DDSs. A more likely cause of the 0.48 kHz offset could be extra signal delay in either the transmit channel or the reference channel due to uneven transmission line length. A difference of about 6 cm between the signal paths could account for

this. To correct for this error, the radar system can be calibrated by subtracting 0.48 kHz from all future beat frequency measurements.

After accounting for the 0.48 kHz offset, the upchirp and downchirp beat frequencies for the targets at R1 & R2 are ±39.7 kHz and ±53.1 kHz. Inserting these values into equation (4.1) suggests that R1 = 4.96 m and R2 = 6.63 m. Note that these calculated ranges are different from the previously measured ranges by 21 cm for R1 and 18 cm for R2, or a mean error of about 19.5 cm.

Several things could contribute to this error, but the likely explanation is that there is a range bias which is dependent on how the distance between the radar system and the target is defined. In this case, target range was measured from the center of the trihedral to the midpoint between the transmit and receive antennas. Defining range this way assumes that the signal originated between the two antennas, neglecting the fact that it was actually produced within the DDSs and travelled through several lengths of transmission line, which may not be equivalent between the two signal paths. If transmission line length within the radar system is unchanged, the resulting 19.5 cm range bias will be constant and can be subtracted from the calculated ranges for R1 and R2.

Even after calibration, range calculations still differ from measured range by about ±1.5 cm. This remaining error could be the result of using a soft measuring tape to measure the distance to the trihedrals, meaning that there could be error in the physical range measurements rather than those obtained from the radar. Another small factor that could contribute to range error is that the data shown in figure 4-4 represents a set of discrete frequency values (not continuous). This means that if the actual beat frequency lies between two discrete points, the nearest frequency element will be selected as the beat frequency. Error resulting from discrete

data will always exist, but it can be minimized by increasing the sampling rate, or by zero-padding when performing FFTs.

The calibration methods described in the preceding paragraphs should be performed when physical changes are made to transmission line length within the radar system. This kind of radar calibration is necessary to account for time the signal spends propagating through the system before it enters free space. Radar calibration helps maintain accuracy in range and velocity measurements and improves the clutter suppression techniques that will be described in chapter 5.

Target Velocity Test Setup & Results

The next tests that were performed were designed to verify that the radar system could accurately measure radial velocity. These tests required that an object with a relatively high velocity pass through the antenna beam at a known angle. Several methods for projecting fast moving objects were considered, but ultimately it was decided that firing reballs (re-useable paintballs) from a paintball gun would provide the simplest and most repeatable experiment. The selected paintball gun was capable of firing the reball with initial velocities of up to 110 m/s (246 mph). However, because muzzle velocity can be adjusted by increasing or decreasing the pressurized-air valve capacity, actual muzzle velocity was unknown.

In the space limited by the test environment, a reball travelling at an average velocity of 92 m/s would be in flight for less than 100 ms before impact. As stated previously, for the oscilloscope to maintain a sampling frequency high enough to satisfy the Nyquist sampling rate, the amount of time that could be recorded was limited to about 100-150 ms. This means that to

record signal data while the reball is in motion, the oscilloscope would need to be triggered at approximately the same time that the reball was fired. To accomplish this, an IR (infrared) sensor was designed and fixed to the barrel of the paintball gun such that when the reball left the barrel it would pass through the IR sensor beam, as seen in figure 4-5.

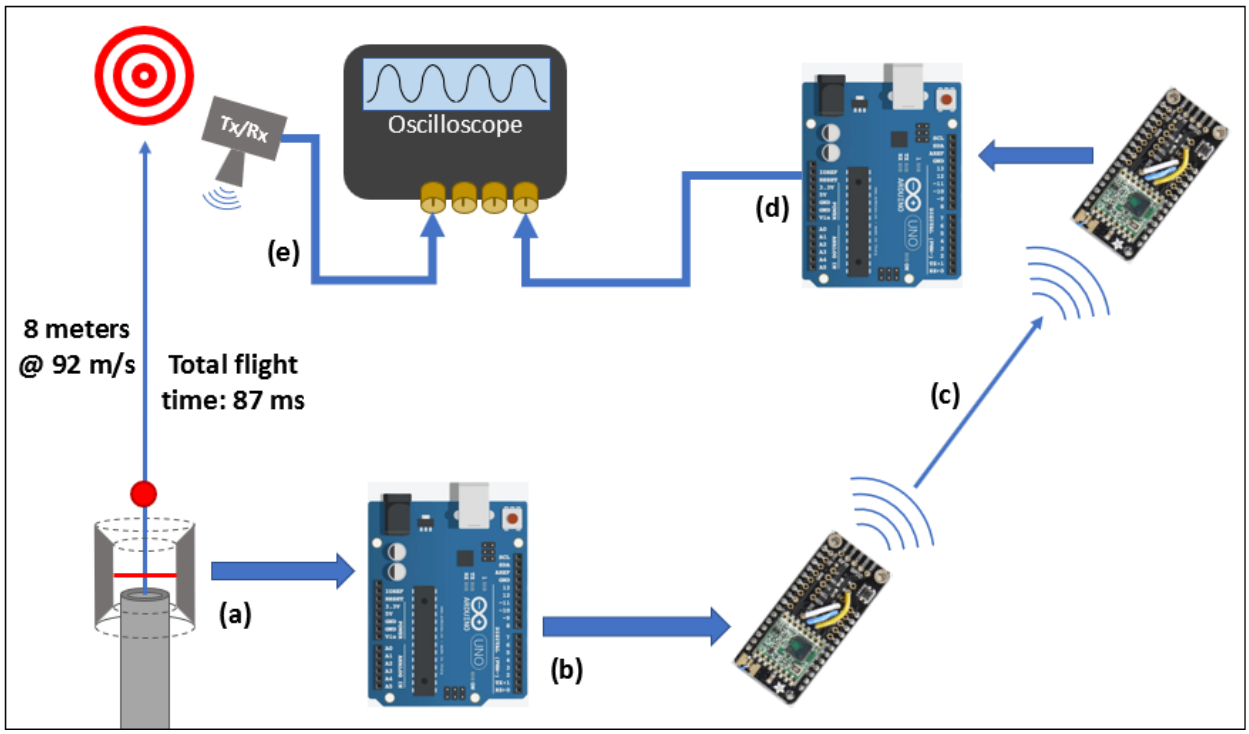

Figure 4-5: Oscilloscope remote trigger system diagram. (a) upon firing, reball passes through IR sensor. (b) an Arduino registers the break in the IR beam and prompts transmitter. (c) 433 MHz signal is transmitted and received. (d) second Arduino triggers oscilloscope to begin recording. Delay between IR sensor event and oscilloscope trigger is approximately 3.4 ms. Reball travels 0.31 m during that time. (e) Oscilloscope begins recording reball return signal data.

The IR sensor was wired to an Arduino Uno board with attached Adafruit Feather 32u4 Radio & RFM69HCW module. Once the Arduino registers a break in the IR sensor beam, a 433 MHz signal is transmitted to an identical receiver that is located next to the oscilloscope. When this signal is picked up at the receiver, a second Arduino sends a signal to one of the

oscilloscope input channels, triggering the oscilloscope to begin recording. The delay time from the firing event until the oscilloscope begins recording is approximately 3.4 ms, corresponding to a distance of about 0.31 meters travelled by the reball.

Because initial reball velocity could not be precisely known, and because inherent differences between reballs could alter their velocity from shot to shot, efforts were made to get a better idea of the range of velocities that could be expected. Assuming the reball will travel towards the radar system at speeds of 80-110 m/s (or 179-246 mph), the Doppler frequency equation (3.3) suggests that frequencies on the range of 58.4-80.3 kHz should be seen.

To confirm this, the radar system was reconfigured with microwave signal generators (instead of DDSs) to operate in CW mode so that target range would be ignored and the only difference between the received signal and the reference signal would be the artificial 3 MHz offset and a Doppler frequency shift due to target velocity. The main differences between this test environment and the test environment used for the previous test is the removal of the two trihedrals and the addition of a sheet that was positioned about 0.5 m in front of the radar system to protect it from the incoming reball (see figure 4-6).

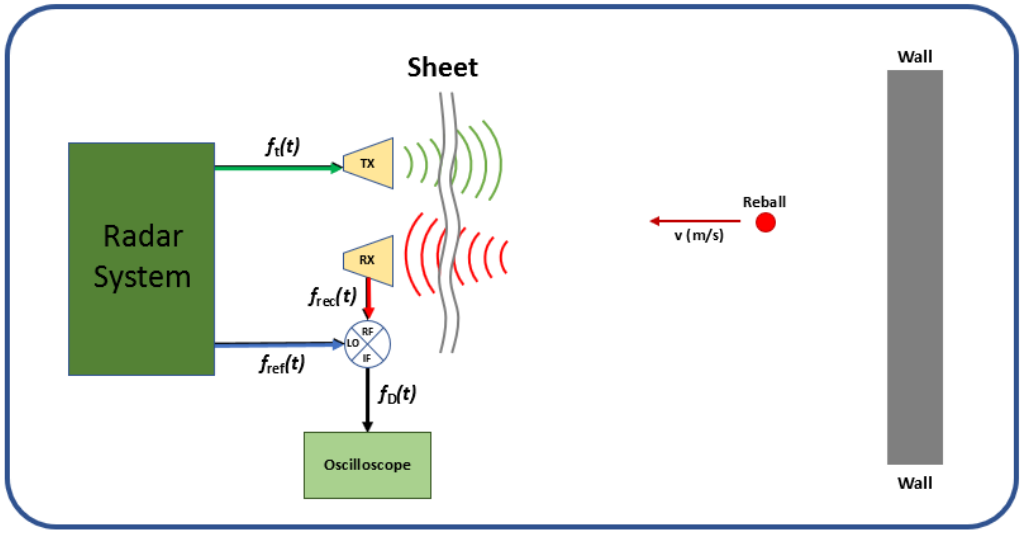

Figure 4-6: CW mode test setup for measuring target velocity while ignoring target range. A sheet is hung on a frame to protect radar system from incoming projectiles while still allowing the transmitted signal to pass through.

The results of this test can be seen in figure 4-7 below. An important note for this shot is that, contrary to most tests, the +3 MHz offset was applied to the reference signal instead of the transmit signal. Therefore, even though a shot fired towards the radar system will always yield a positive Doppler frequency, we see that it appears below the 3 MHz offset because of how that offset was applied.

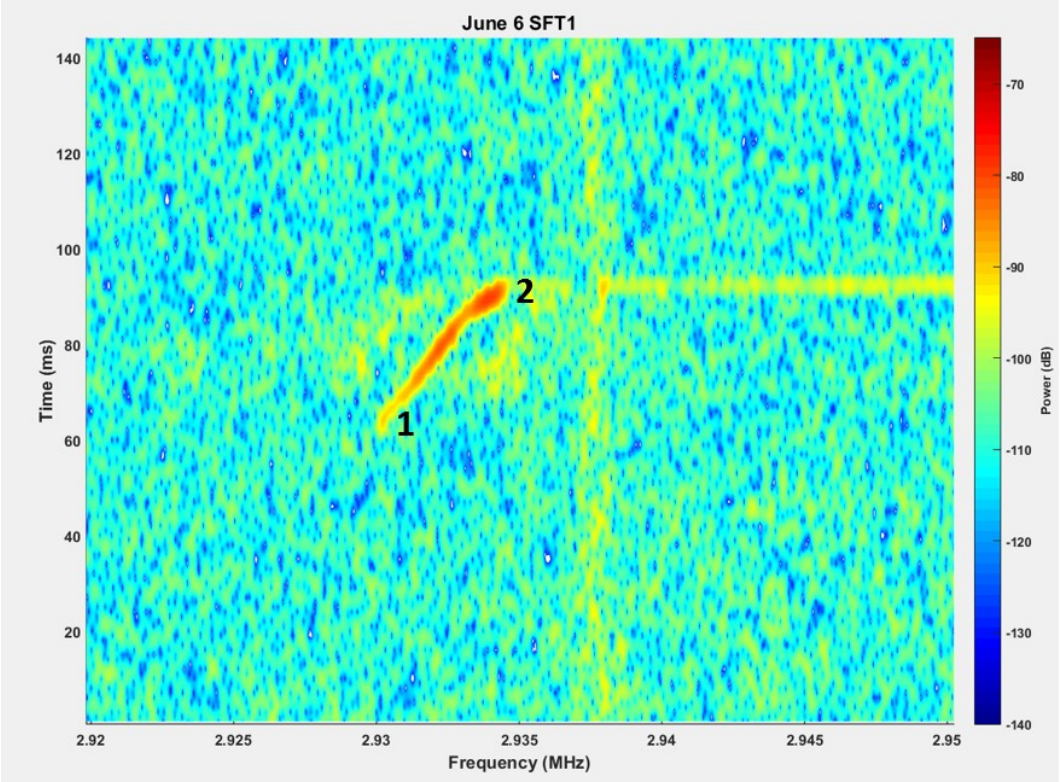

Figure 4-7: Surface plot of frequency spectrum that results from a shot fired towards (SFT) the radar system. As time increases, Doppler frequency moves closer to the 3 MHz offset, indicating that the reball is decelerating. The reball is initially detected (1) at 64 ms with a Doppler frequency of 69.8 kHz, which corresponds to a velocity of 95.6 m/s. Impact occurs at about 92 ms (2) when the reball has a Doppler frequency of 66.1 kHz, suggesting a final velocity of 90.5 m/s. If deceleration is constant, the average velocity between points 1 and 2 is 93.05 m/s, and distance travelled during 28 ms of observation is about 2.61 m.

According to the data shown in figure 4-7, the reball was first detected 64 ms after the shot was fired and had a Doppler frequency (f_D) of [3 $MHz - 2.9302\ MHz$] or 69.8 kHz, which corresponds to a velocity of 95.57 m/s. At time of impact (appr. 92 ms), f_D had dropped to 66.1 kHz, corresponding to a velocity of 90.5 m/s. This means that over the course of 28 ms, the reball's speed decreased by 5.07 m/s, a deceleration rate of about 0.181 m/s/ms (meters per second per millisecond). Based on the 28 ms of observed flight-time, deceleration appears to be approximately linear with respect to time. Assuming that is the case, the muzzle velocity can be

calculated by extrapolating backwards from the time the reball was initially detected. Doing so yields a muzzle velocity of 107.15 m/s and an overall average velocity of 98.83 m/s.

Data was collected for two additional shots with the radar system under the same configuration and operating in CW mode. Using the same method described above, average velocities for these shots were calculated to be approximately 101.04 m/s and 96.41 m/s. Relevant target data for all three shots can be seen in table 4-1 below. The results of these tests provide a baseline for expected reball velocities in future tests and will help to verify system accuracy when calculating range and velocity using target beat frequency.

Table 4-1: Reball firing data collected during three separate shots while operating in CW mode.

	Shot 1	**Shot 2**	**Shot 3**
t_{init}	64 ms	65 ms	63 ms
f_{D_init}	69.8 kHz	68.1 kHz	71.1 kHz
v_{init}	95.57 m/s	93.24 m/s	97.35 m/s
t_{fin}	92 ms	93 ms	86 ms
f_{D_fin}	66.1 kHz	64.6 kHz	68.0 kHz
v_{fin}	90.5 m/s	88.45 m/s	93.11 m/s
$max\ range$	2.61 m	2.19 m	2.54 m
$deceleration$	0.1809 m/s/ms	0.1711 m/s/ms	0.1845 m/s/ms
v_{muzzle}	107.15 m/s	104.37 m/s	108.98 m/s
v_{avg}	98.83 m/s	101.04 m/s	96.41 m/s

Chapter 5. Measuring Moving Target Range & Velocity

To measure both range and velocity of a moving target, the radar system was reconfigured as shown in the system diagram in figure 1. For this test, the DDSs were programmed to produce triangular waveforms comprised of 1 ms upchirps and 3 ms downchirps. The bandwidth of the transmit signal in this case was 240 MHz, and the center frequency was approximately 108.36 GHz.

With no trihedrals in the scene, a reball was fired directly away from the radar system. Various stationary objects within the room such as tables, chairs, and the back wall provided significant backscatter which is clearly visible in the collected data, plotted in figure 5-1.

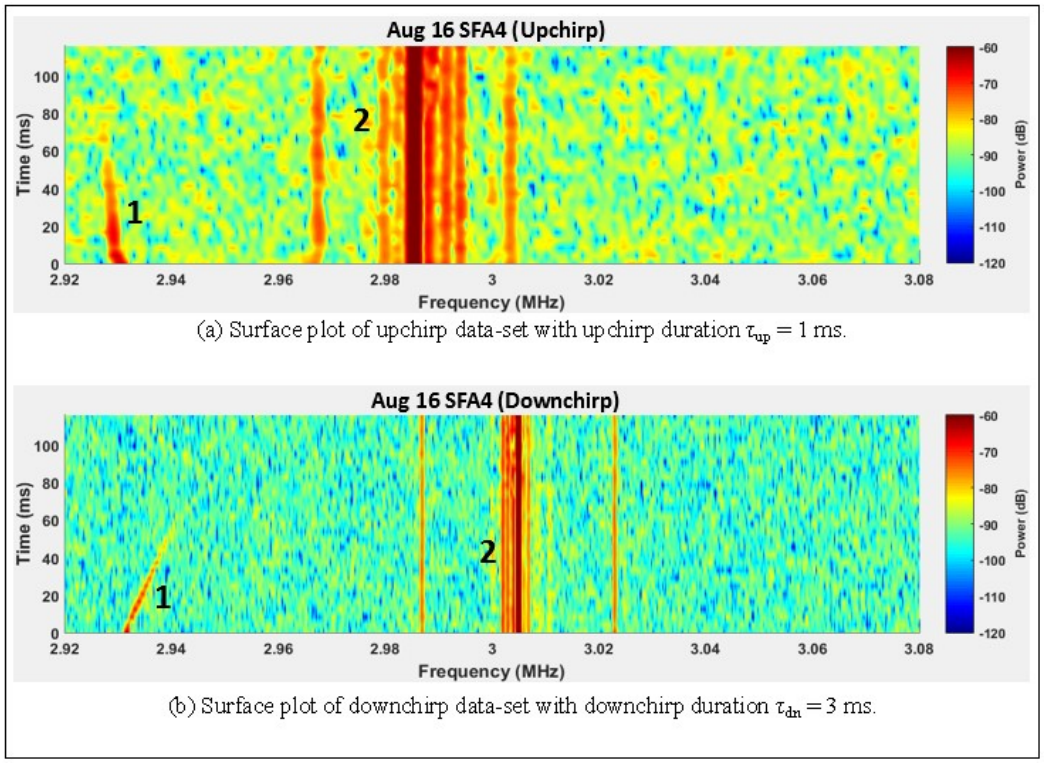

(a) Surface plot of upchirp data-set with upchirp duration $\tau_{up} = 1$ ms.

(b) Surface plot of downchirp data-set with downchirp duration $\tau_{dn} = 3$ ms.

Figure 5-1: Surface plots of data collected over 115 ms resulting from a shot fired away (SFA) from the radar system. In figures (a) and (b), point 1 indicates the detection of the reball, while point 2 shows return signals from various stationary objects (static clutter). The upchirp and downchirp static clutter beat frequencies are not symmetric about 3 MHz in this test because $\tau_{up} \neq \tau_{dn}$.

Both plots (a) and (b) in figure 5-1 show the return signals from the reball (marker 1) and from the static clutter in the room (marker 2). To show how altering bandwidth and chirp duration can affect target beat frequency, the return signal from the stationary objects will be examined. Note that, unlike the results portrayed in figure 4-4 where upchirp and downchirp durations were equivalent, the upchirp and downchirp beat frequencies here are not symmetric about the 3 MHz offset. With differing chirp durations ($\tau_{up} \neq \tau_{dn}$), the upchirp and downchirp beat frequency equations (3.5) and (3.6) become:

$$f_{b\_up} = -\frac{2BR}{\tau_{up}c} - \frac{2vf_c}{c} \tag{5.1}$$

$$f_{b\_dn} = \frac{2BR}{\tau_{dn}c} - \frac{2vf_c}{c} \tag{5.2}$$

This means that for static targets ($v = 0$), f_{b_up} is not equal to $-f_{b\_dn}$, but they will instead be scaled versions of each other proportional to the ratio of τ_{up} to τ_{dn}. In this case, with $\tau_{dn} = 3\tau_{up}$, we find that, for stationary targets, $f_{b\_up} = -3f_{b\_dn}$. This relationship is easier to see in figure 5-2, which is a closeup of the frequency spectrum of the data set from figure 5-1.

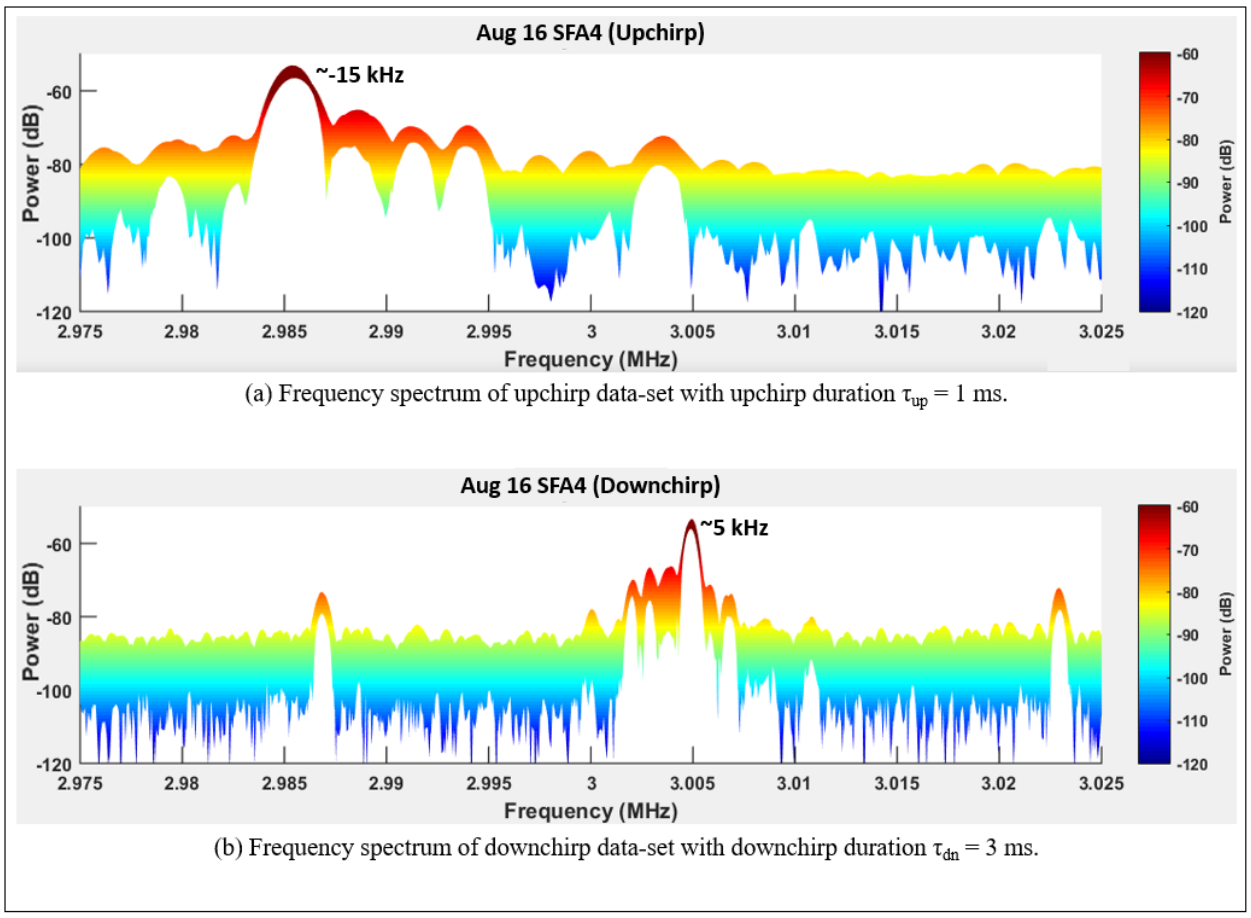

(a) Frequency spectrum of upchirp data-set with upchirp duration τ_{up} = 1 ms.

(b) Frequency spectrum of downchirp data-set with downchirp duration τ_{dn} = 3 ms.

Figure 5-2: Frequency spectrum of static clutter for the 1 ms upchirp data set (a) and the 3 ms downchirp data set (b). The main peaks, labelled -15 kHz in (a) and 5 kHz in (b) are beat frequencies from the same target. Having beat frequencies $f_{b\_up} = -3f_{b\_dn}$, implies that $\tau_{dn} = 3\tau_{up}$.

The strongest signal in subplot (a) of figure 5-2, located at 2.985 MHz, has a beat frequency (f_{b_up}) of -15 kHz, while the corresponding peak in subplot (b), located at 3.005 MHz, has a beat frequency (f_{b_dn}) of +5 kHz. If each beat frequency and associated chirp duration (1 ms for upchirp and 3 ms for downchirp) is plugged into the range equation (4.1), it is determined that both beat frequencies resulted from the same object at a range of 9.37 m. This is a good example of how static target beat frequencies can be manipulated by simply increasing or decreasing chirp duration. The implications of this will be discussed in chapter 6.

Focusing now on the reball, figure 5-3 is a close-up of the portion of the frequency spectrum containing the reball echo signal beat frequency.

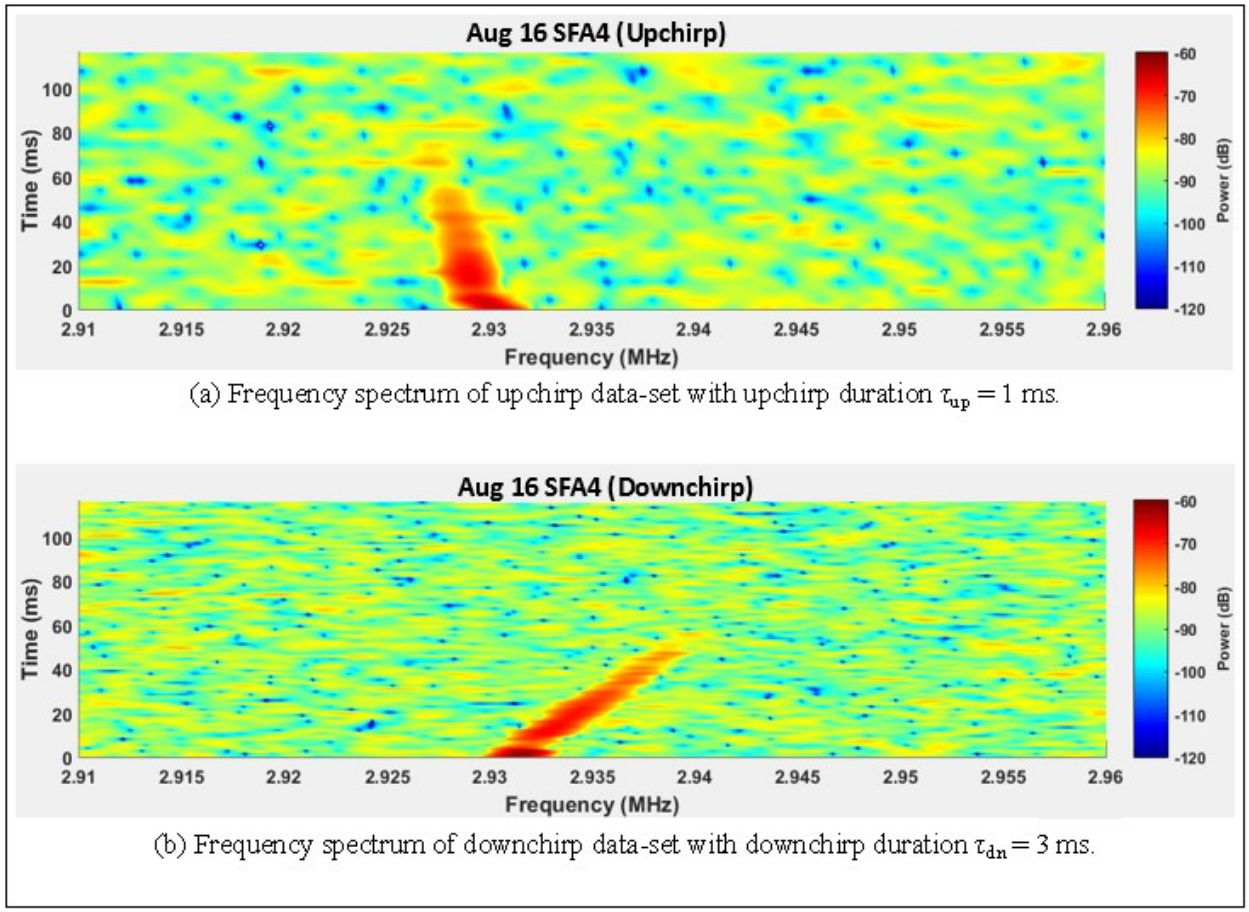

Figure 5-3: Reball upchirp beat frequency vs downchirp beat frequency.

By observation of subplots (a) and (b) in the figure, the beat frequency can be determined throughout the observed flight time of the reball. Although the change in beat frequency appears to be continuous over time, it is important to remember that between every 1 ms upchirp data sample, there is a 3 ms gap when a downchirp was being transmitted (and vice-versa).

It was shown in Chapter 2 that for moving targets, when transmitting a triangular waveform, the upchirp and downchirp beat frequencies can be used together to solve for the two unknown variables, range and velocity. This was somewhat of a simplification; it fails to

account for the gap that exists between chirps because upchirps and downchirps cannot be transmitted simultaneously. If chirp durations (τ_{up} & τ_{dn}) are very small, it could be assumed that intermediate changes in target range and velocity will be negligible, but for greater accuracy, the following method can be applied.

Figure 5-4 shows how the upchirp and downchirp beat frequency data samples alternate back and forth over time. These beat frequencies can be parsed into two different arrays—an upchirp array and a downchirp array—where each array contains either even or odd beat frequency indices, depending on whether an upchirp or downchirp was sampled first. To illustrate this method, suppose we wanted to use these data to determine the reball range and velocity 20 ms after it was fired. An upchirp beat frequency sample $f_{b\_up}(n+1)$ was recorded at approximately 20 ms, but the two closest downchirp beat frequency samples $f_{b\_dn}(n)$ & $f_{b\_dn}(n+2)$ occurred at about 18 ms and 22 ms, respectively.

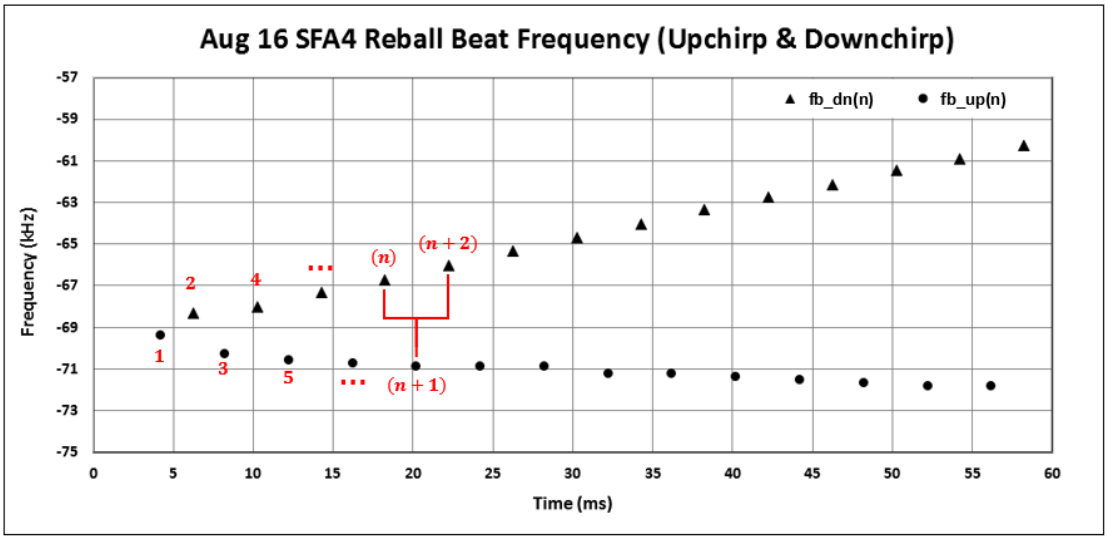

Figure 5-4: Reball return signal beat frequency vector. The upchirp and downchirp beat frequencies shown here correspond to the data shown in figure 5-3a and 5-3b, respectively. The values in red are the index numbers for that transmit/receive event. Three time-adjacent data points are required to calculate range and velocity at a single point in time.

Because we have knowledge of the beat frequency immediately before and after the time of interest, we can use $f_{b\_dn}(n)$ & $f_{b\_dn}(n+2)$ to approximate what the downchirp beat frequency would have been, had a downchirp also been sampled at 20 ms. This is done by taking the average of $f_{b\_dn}(n)$ & $f_{b\_dn}(n+2)$, which is done mathematically as follows:

Begin with $f_{b\_dn}(n)$ & $f_{b\_dn}(n+2)$,

$$f_{b\_dn}(n) = \frac{2B(R_n)}{\tau_{dn}c} - \frac{2(v_n)f_c}{c} \tag{5.3}$$

$$f_{b\_dn}(n+2) = \frac{2B(R_{n+2})}{\tau_{dn}c} - \frac{2(v_{n+2})f_c}{c} \tag{5.4}$$

Where R_n, R_{n+2}, v_n and v_{n+2} are the unknown range and radial velocity of the reball at the time samples (n) and $(n+2)$ were taken. The average of equations (5.3) and (5.4) is found by adding them together and dividing by 2.

$$\frac{f_{b\_dn}(n)+f_{b\_dn}(n+2)}{2} = \frac{\frac{2B(R_n)}{\tau_{dn}c} - \frac{2(v_n)f_c}{c} + \frac{2B(R_{n+2})}{\tau_{dn}c} - \frac{2(v_{n+2})f_c}{c}}{2}$$

$$= \frac{\left[\frac{2B(R_n)}{\tau_{dn}c} + \frac{2B(R_{n+2})}{\tau_{dn}c}\right] - \left[\frac{2(v_n)f_c}{c} + \frac{2(v_{n+2})f_c}{c}\right]}{2}$$

$$= \frac{\frac{2B}{\tau_{dn}c}[(R_n)+(R_{n+2})]}{2} - \frac{\frac{2f_c}{c}[(v_n)+(v_{n+2})]}{2}$$

$$= \frac{2B}{\tau_{dn}c}\frac{[(R_n)+(R_{n+2})]}{2} - \frac{2f_c}{c}\frac{[(v_n)+(v_{n+2})]}{2} \tag{5.5}$$

At this point, if we assume that changes in range and velocity are approximately linear (small acceleration) over the 4 ms interval between samples (n) & $(n+2)$ —as data collected

up to that point would lead us believe—and if we acknowledge that the midpoint between the two samples is the same point in time that sample $(n+1)$ took place, then the following statements should be true:

$$R_{n+1} \cong \frac{[(R_n)+(R_{n+2})]}{2} \qquad \& \qquad v_{n+1} \cong \frac{[(v_n)+(v_{n+2})]}{2} \tag{5.6}$$

Where R_{n+1} and v_{n+1} are the range and radial velocity of the reball at the time that the beat frequency sample $f_{b\_up}(n+1)$ was taken. Therefore, if we plug (5.6) into (5.5), the approximate downchirp beat frequency $f_{b\_dn}(n+1)$ that would be expected if a downchirp had been sampled at the same time as $f_{b\_up}(n+1)$, could be defined as:

$$f_{b\_dn}(n+1) = \frac{f_{b\_dn}(n)+f_{b\_dn}(n+2)}{2} = \frac{2B(R_{n+1})}{\tau_{dn}c} - \frac{2(v_{n+1})f_c}{c} \tag{5.7}$$

Which can be used in conjunction with the equation for the upchirp beat frequency, $f_{b\_up}(n+1)$, defined as:

$$f_{b\_up}(n+1) = -\frac{2B(R_{n+1})}{\tau_{up}c} - \frac{2(v_{n+1})f_c}{c} \tag{5.8}$$

Note that the negative sign associated with the range component in (5.8) is due to $f_{rec}(t)$ being less than $f_t(t)$ during an upchirp (see figure 7).

There are now two equations (5.7) & (5.8) which refer to upchirp and downchirp beat frequencies for a single point in time. By repeating this process for each set of adjacent upchirps and downchirps, approximate beat frequency values can be found for each gap that resulted from alternating between upchirps and downchirps. A plot of the complete upchirp and downchirp beat frequency sets can be seen in figure 5-5.

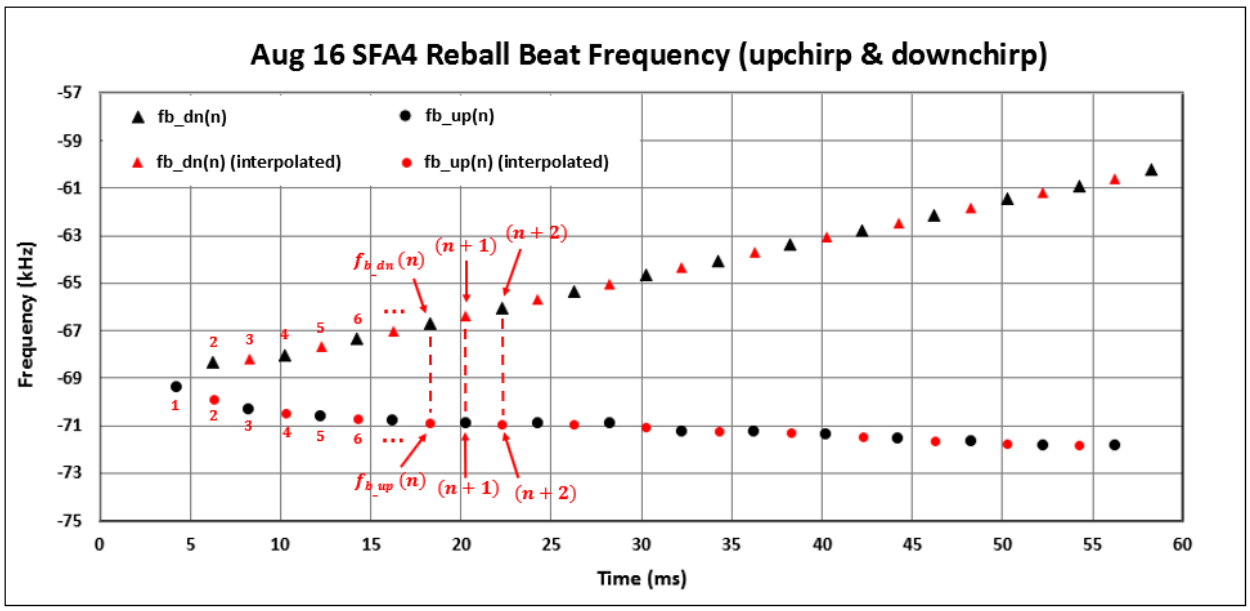

Figure 5-5: A plot of upchirp and downchirp beat frequencies, similar to that found in figure 5-4. Measured values are indicated by black symbols, while interpolated beat frequencies are indicated by red symbols. Excluding first and last samples, there are now corresponding upchirp and downchirp beat frequency values for each time interval.

Since the velocity components of both equations are equivalent, if we take the difference between the upchirp and downchirp beat frequencies, the velocity terms will cancel, and the only remaining terms will be the beat frequency components due to range. The difference between $f_{b\_dn}(n+1)$ & $f_{b\_up}(n+1)$ will be referred to as $\Delta f_b(n+1)$, which is defined as follows:

$$\Delta f_b(n+1) = f_{b\_dn}(n+1) - f_{b\_up}(n+1)$$

$$= \left(\frac{2B(R_{n+1})}{\tau_{dn}c} - \frac{2(v_{n+1})f_c}{c}\right) - \left(-\frac{2B(R_{n+1})}{\tau_{up}c} - \frac{2(v_{n+1})f_c}{c}\right)$$

$$= \frac{2B(R_{n+1})}{\tau_{dn}c} + \frac{2B(R_{n+1})}{\tau_{up}c} - \left(\frac{2(v_{n+1})f_c}{c} - \frac{2(v_{n+1})f_c}{c}\right)$$

$$= \frac{2B(R_{n+1})}{\tau_{dn}c} + \frac{2B(R_{n+1})}{\tau_{up}c}$$

$$= \frac{2B(R_{n+1})}{c}\left(\frac{1}{\tau_{dn}} + \frac{1}{\tau_{up}}\right)$$

$$\Delta f_b(n+1) = \frac{2B(R_{n+1})}{c}\left(\frac{\tau_{up}+\tau_{dn}}{\tau_{dn}\tau_{up}}\right) \tag{5.9}$$

Note here that the only unknown variable in equation (5.9) is the reball range (R_{n+1}). Rearranging equation (5.9) to solve for range gives:

$$R_{n+1} = \Delta f_b(n+1)\frac{c}{2B}\left(\frac{\tau_{dn}\tau_{up}}{\tau_{up}+\tau_{dn}}\right) \tag{5.10}$$

Now, since range is known, reball radial velocity (v_{n+1}) can be determined by simply evaluating equation (5.8), using the known range in place of R_{n+1}, and solving in terms of v_{n+1}, which results in the following equation:

$$v_{n+1} = -\frac{\left(f_{b\_up}(n+1)+\frac{2B(R_{n+1})}{\tau_{up}c}\right)c}{2f_c} \tag{5.11}$$

Alternatively, velocity can be determined independent of range by taking the average of the upchirp and downchirp beat frequencies at any given time. Doing so will cause the range dependent terms to cancel, leaving only the terms dealing with reball velocity. If upchirp and downchirp durations are not equivalent, as is the case for this data set, then a weighted average is required. This is found by factoring the ratio of upchirp duration to downchirp duration into the beat frequency equations before adding them together, and then dividing their sum by the total triangular wave form duration, as follows:

$$f_{b\_w\_avg}(n+1) = \frac{f_{b\_dn}(n+1)\left(\frac{\tau_{dn}}{\tau_{up}}\right)+f_{b\_up}(n+1)}{\tau_{dn}+\tau_{up}} \tag{5.12}$$

where τ_{dn} & τ_{up} are in milliseconds.

Applying equation (5.12) to the current test data, recall that $\tau_{dn} = 3\ ms$ and $\tau_{up} = 1\ ms$. Then $\tau_{dn}/\tau_{up} = 3$, and $\tau_{dn} + \tau_{up} = 4\ ms$. With $\tau_{dn} = 3\tau_{up}$, the downchirp beat frequency defined in equation (5.7) can be rewritten in terms of τ_{up}, resulting in:

$$f_{b\_dn}(n+1) = \frac{2B(R_{n+1})}{3\tau_{up}c} - \frac{2(v_{n+1})f_c}{c} \tag{5.13}$$

The weighted average of the upchirp and downchirp beat frequencies can now be found by inserting equations (5.13) and (5.8) into equation (5.12).

$$f_{b\_w\_avg}(n+1) = \frac{3f_{b\_dn}(n+1)+f_{b\_up}(n+1)}{4}$$

$$= \frac{3\left(\frac{2B(R_{n+1})}{3\tau_{up}c} - \frac{2(v_{n+1})f_c}{c}\right)+\left(-\frac{2B(R_{n+1})}{\tau_{up}c} - \frac{2(v_{n+1})f_c}{c}\right)}{4}$$

$$= \frac{\left(\frac{2B(R_{n+1})}{\tau_{up}c} - \frac{6(v_{n+1})f_c}{c}\right)+\left(-\frac{2B(R_{n+1})}{\tau_{up}c} - \frac{2(v_{n+1})f_c}{c}\right)}{4}$$

$$= \frac{-\frac{6(v_{n+1})f_c}{c} - \frac{2(v_{n+1})f_c}{c}}{4}$$

$$f_{b\_w\_avg}(n+1) = -\frac{2(v_{n+1})f_c}{c} \tag{5.14}$$

Or equivalently,

$$\frac{\tau_{dn}f_{b\_dn}(n+1)+\tau_{up}f_{b\_up}(n+1)}{\tau_{dn}+\tau_{up}} = -\frac{2(v_{n+1})f_c}{c} = f_D(n+1) \tag{5.15}$$

Where $f_D(n+1)$ is defined to be the Doppler frequency of the reball at the time sample $(n+1)$ was taken.

Equations (5.14) & (5.15) make it apparent that by taking the weighted average of the upchirp and downchirp beat frequencies, radial velocity can be determined without regards to range. And since values are known for every variable other than v_{n+1}, equation (5.15) can be rearranged to solve for radial velocity.

$$v_{n+1} = -\left(\frac{\tau_{dn} f_{b\_dn}(n+1) + \tau_{up} f_{b\_up}(n+1)}{\tau_{dn} + \tau_{up}}\right)\frac{c}{2f_c} \tag{5.16}$$

By applying equations (5.10) and (5.16) to each beat frequency sample in figure 5-5, range and radial velocity can be determined for each upchirp/downchirp beat frequency pair. Note that the first and last beat frequency samples cannot be used because each interpolated upchirp (or downchirp) was dependent on both a prior and subsequent upchirp (or downchirp) to have occurred. Therefore, the first and last beat frequency samples do not directly result in range or velocity measurements. The range and velocity values that could be determined for the current test are plotted in figure 5-6.

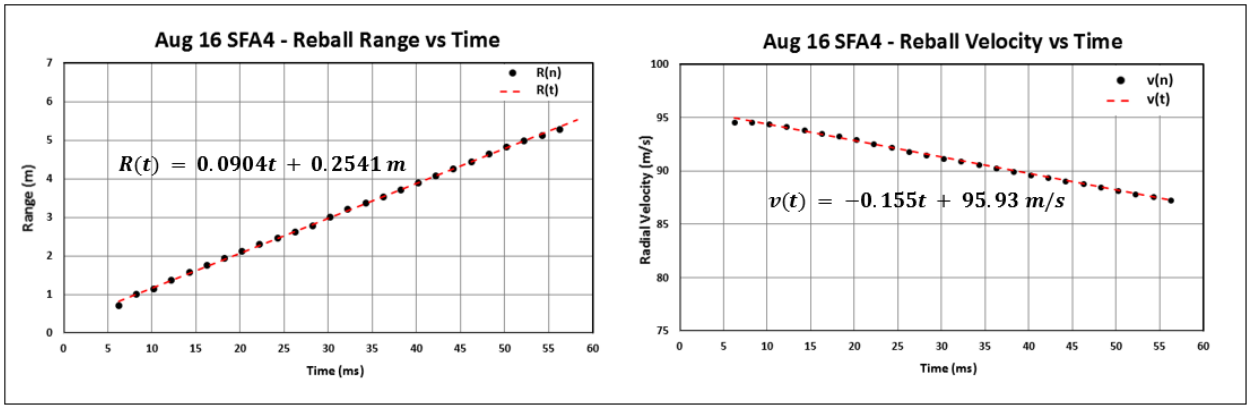

Figure 5-6: Reball range and radial velocity over time. Each plot is overlayed with a 1st order trendline and associated line equation. Taking the derivative of the range function indicates an average velocity of 90.4 m/s, while taking the derivative of the velocity function suggests an accelleration rate of -0.155 m/s/ms.

Both plots in figure 5-6 are overlaid with a 1st order trendline and associated line equation. Taking the derivative of the range function found in the plot on the left, results in a velocity of 90.4 m/s, which would be the average velocity of the reball over the observed flight time. That value closely matches the average velocity of 90.9 m/s that can be derived from the plot on the right by adding the final and initial velocity measurements and dividing their sum by 2. By taking the derivative of the velocity function, acceleration is determined to be -0.155 m/s/ms.

For this test, reball beat frequency, range and velocity were all found during the post-processing phase from data that had been previously recorded. However, the process described above could also be implemented in real-time because the range and velocity for any given sample can be calculated as soon as the next upchirp or downchirp occurs. If this process were actually happening in real-time, the exact delay would depend mainly on upchirp and downchirp duration (τ_{up} & τ_{dn}), and in the case that $\tau_{up} \neq \tau_{dn}$, it would also depend on whether an upchirp or downchirp was currently being transmitted.

Assuming the fast-time FFT is performed on data collected over an entire upchirp or downchirp, the time of the resulting beat frequency, range and velocity measurements will correspond to the time at the midpoint of the associated chirp, or $t = t_{start} + \tau/2$. But before the range and velocity at that time can be determined, the following chirp must be completed, and the beat frequency measured. This means that the range and velocity information for any given beat frequency sample would not be available until $[t + \tau_{up}/2 + \tau_{dn}]$ for an upchirp, or $[t + \tau_{dn}/2 + \tau_{up}]$ for a downchirp. However, projectile motion is very predictable so future target range and velocity could be approximated before additional data are processed, and then those data could be used to either verify projected range and velocity, or correct any error.

If real-time processing is not necessary for a particular radar application, an alternative post-processing method can be used. For instance, if the recorded data for an entire event were analyzed together instead of only looking at three consecutive beat frequency samples, more accurate range and velocity information could be obtained and expressed as a function of time. The benefit of this is that good approximations of range and velocity can be given at every point in time for the observed event. Also, based on target range and velocity trends, anomalies can be ignored and intermittent signal data that could not be recovered due to noise or interference can be interpolated.

For the current test, since it took place in a low clutter environment and the reball signal was easily detectable in both the upchirp and downchirp data sets, little would be gained by implementing the post processing method just described. The range, velocity and beat frequency trends in figures 5-4 and 5-6 are already linear and consistent over the observed time. But to show how these trends could be used, see figure 5-7 below.

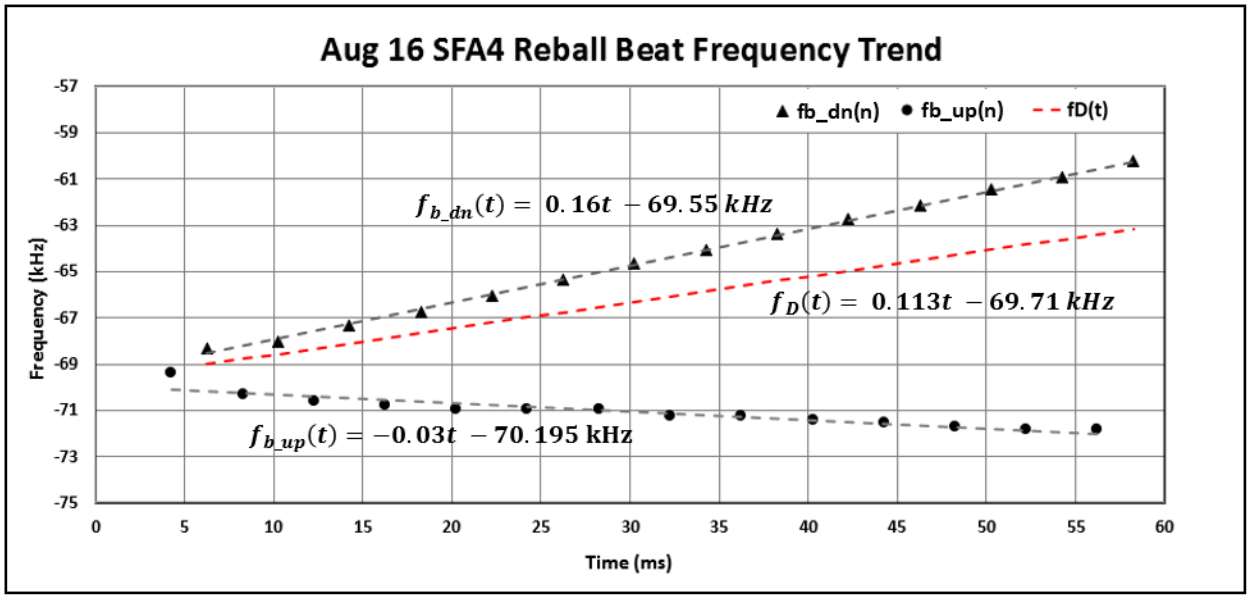

Figure 5-7: 1st Order equations have been fitted to the upchirp and downchirp beat frequencies, to show how the reball beat frequency changed over time. By taking the weighted average of the beat frequency trendlines, the reball Doppler frequency can be determined as a function of time.

In figure 5-7, the upchirp and downchirp beat frequencies are expressed by 1st order equations, $f_{b\_up}(t)$ & $f_{b\_dn}(t)$, to describe how they both change as a function of time. If the change in beat frequency did not appear to be linear, the functions could be altered to include higher order terms to make the line-fit more accurate. The red dashed line in the figure shows the reball Doppler frequency as a function of time, denoted as $f_D(t)$. This function was determined using the same reasoning that led to equation (5.15), which was by taking the weighted average of the upchirp and downchirp beat frequencies at any given time. When applied to a function over a continuous time interval rather than a finite vector of discrete elements, equation (5.15) becomes:

$$f_D(t) = \frac{3f_{b\_dn}(t)+f_{b\_up}(t)}{4} = -\frac{2v(t)f_c}{c} \tag{5.17}$$

Where $v(t)$ is the reball velocity as a function of time. By solving equation (5.17) for $v(t)$, velocity can be determined at any time during the 50 ms that the reball signal was detected.

$$v(t) = -\frac{cf_D(t)}{2f_c} \tag{5.18}$$

Range can be determined from the functions in figure 5-7 in two different ways. The first is analogous to the process that led to equation (5.10), which was used when dealing with discrete vectors. In continuous or discrete time, taking the difference between the upchirp and downchirp beat frequencies leaves only the beat frequency component due to range because the Doppler frequency component will be the same in both. The previously defined vector $\Delta f_b(n)$ can be adapted to continuous time as the function $\Delta f_b(t)$, and defined to be the difference between $f_{b\_dn}(t)$ & $f_{b\_up}(t)$.

$$\Delta f_b(t) = f_{b\_dn}(t) - f_{b\_up}(t) \tag{5.19}$$

Using equation (5.19), a range equation comparable to equation (5.10) can be defined as:

$$R(t) = \frac{\Delta f_b(t)}{2B}\left(\frac{\tau_{dn}\tau_{up}}{\tau_{up}+\tau_{dn}}\right) \tag{5.20}$$

Where the ratio $(\tau\_dn\ \tau\_up)/(\tau\_up + \tau\_dn)$ is the factor that accounts for differing upchirp and downchirp durations.

The second way to find R(t) is by recognizing that Doppler frequency is a component of beat frequency which can be removed simply by subtracting $f_D(t)$ from $f_{b\_up}(t)$ or $f_{b\_dn}(t)$. In doing this, we are left only with the beat frequency component due to range, so a continuous time form of the range equation (4.1) is appropriate to use here. Define the range component of beat frequency for upchirps and downchirps as $f_{bR\_up}(t)$ & $f_{bR\_dn}(t)$.

$$f_{bR\_up}(t) = f_{b\_up}(t) - f_D(t) \tag{5.21}$$

$$f_{bR\_dn}(t) = f_{b\_dn}(t) - f_D(t) \tag{5.22}$$

After inserting (5.21) & (5.22) into the range equation in place of f_b, equation (4.1) becomes:

$$R(t) = \frac{f_{bR\_dn}(t)c\tau_{dn}}{2B} = -\frac{f_{bR\_up}(t)c\tau_{up}}{2B} \tag{5.23}$$

Where the negative sign on the right side of (5.23) is the result of subtracting the Rx signal from the Tx signal, which has a higher frequency during an upchirp (see figure 3-3).

Now, with range and velocity expressed as functions of time in (5.18) and (5.23), not only can both parameters be determined throughout the observation time of the target, but good approximations can also be made about range and velocity after the target is no longer detectable.

Chapter 6. Static Clutter Suppression

Spectral Isolation

The previously discussed methods of obtaining the range and velocity of a moving target work well as long as the echo signals from static clutter do not yield the same total beat frequency as the moving target of interest. When this occurs, the moving target signal beat frequency can become obscured. Looking again at the beat frequency equation (3.4),

$$f_b = \frac{2BR}{\tau c} + f_D$$

we see that if the first term (the contribution due to range) is much larger than the second term, the Doppler frequency shift (f_D) becomes less significant, meaning that stationary targets and moving targets will have very similar beat frequencies and be more difficult to differentiate.

However, by manipulating the signal bandwidth and chirp duration, the range component can be reduced, giving objects with no velocity ($f_D = 0$) a small beat frequency. But for targets with a relatively high radial velocity, f_D can be much larger than the first term, therefore, these targets will have a much higher beat frequency causing them to become spectrally isolated (separated in frequency) from the static clutter, as illustrated in figure 6-1 below.

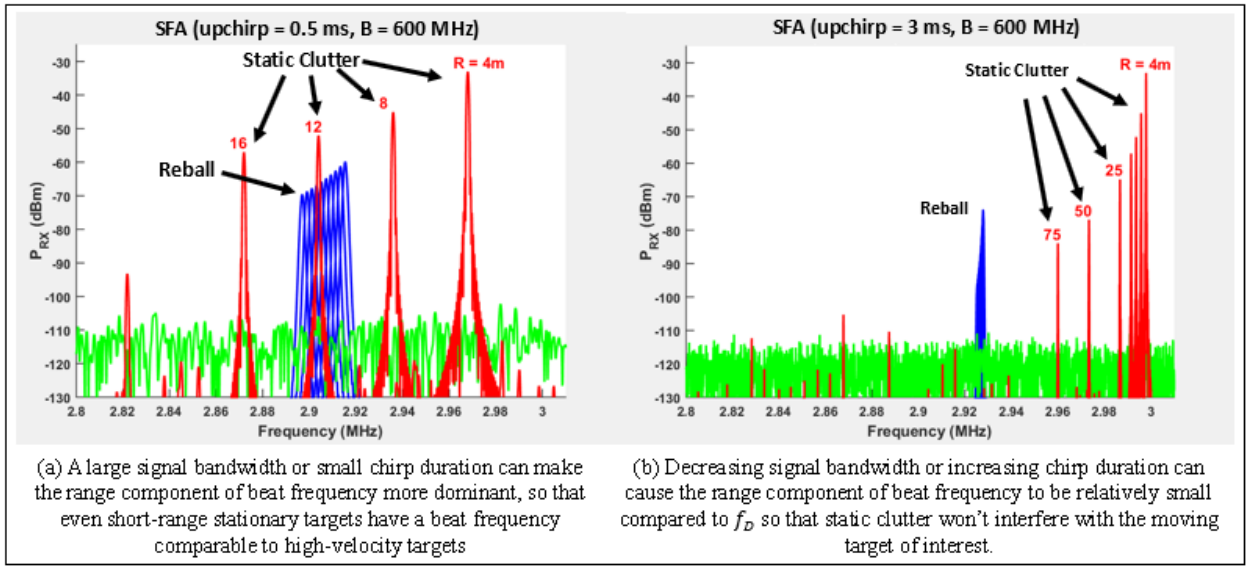

(a) A large signal bandwidth or small chirp duration can make the range component of beat frequency more dominant, so that even short-range stationary targets have a beat frequency comparable to high-velocity targets

(b) Decreasing signal bandwidth or increasing chirp duration can cause the range component of beat frequency to be relatively small compared to f_D so that static clutter won't interfere with the moving target of interest.

Figure 6-1: MATLAB simulation of a reball being fired away from the radar system with initial range of 0.5 m and a constant velocity of 90 m/s, in the presence of static clutter. Simulation compares the series of beat frequencies from stationary and moving targets under varying transmit signal bandwidth and chirp duration parameters. The reball signal spread in (a) and (b) is due to the reball beat frequency changing over time as range increases.

Figure 6-1 is a MATLAB simulation showing the frequency spectrum you might see if a reball were fired away from the radar system at an initial range of 0.5 m and a constant velocity of 90 m/s. The reball signal appears multiple times in each figure because data for ten consecutive upchirps is being plotted and the reball range is increasing over time. In figure 6-1a, the signal bandwidth (B) is 600 MHz, and the upchirp duration (τ_{up}) is 0.5 ms. Stationary objects are detected at ranges of 4, 8, 12, and 16 meters, each of which has a radar cross section (RCS) about 56 dB larger than the reball. It is apparent from figure 6-1a that the 12 m point target has a beat frequency similar to that of the reball. The signal overlap from the stationary target obscures the reball return signal, making it more difficult to extract accurate range or velocity information from the reball.

However, by reducing the bandwidth to 240 MHz and increasing the chirp duration of the transmitted signal to 3 ms, the range component of beat frequency becomes considerably

smaller. As a result, the return signals from the stationary clutter are compressed more towards the 3 MHz reference. The range component of the reball beat frequency is also affected but, because of its large Doppler frequency, the reball signal becomes spectrally isolated from the static clutter (see figure 6-1b). In this case, even stationary objects 75 m away have a beat frequency too small to interfere with the reball signal, and the return signal from more distant objects would likely be too faint to obstruct the echo signal from the reball.

Changing the bandwidth and chirp duration in this manner may have unwanted side-effects. For instance, reducing signal bandwidth also degrades range resolution ΔR (see appendix B for range resolution equation), which can make it impossible to distinguish between objects that are too close together. Additionally, an increase in chirp duration means more time will pass between subsequent chirps, ultimately decreasing the rate at which target information is obtained. Whether or not these side-effects are acceptable depends on the radar application. When range resolution and data rate cannot be sacrificed, other steps may need to be taken to prevent the moving target echo signal from being lost in the clutter. One such method for increasing moving target detectability is static clutter suppression via signal processing, which will be discussed in the following section.

Static Clutter Suppression

The way in which clutter suppression was implemented for this project requires the transmitted signal to be a triangular waveform with equal duration upchirps and downchirps, and for a frequency offset (Δf_c) to exist between the transmitted signal and the reference signal. The frequency offset should be chosen so that it is greater than the maximum possible beat frequency which could be obtained from any target within the antenna beam. When this is the case, the

return signal from all stationary objects will yield two beat frequencies (f_{b_up} & f_{b_dn}) which will appear at equal distances above and below the frequency offset (see figure 3-6).

However, the added Doppler shift of moving targets, which does not change signs with the alternating upchirp/downchirp cycle, ensures that moving target signals will not be perfectly mirrored across the frequency offset. In fact, if the Doppler frequency shift is large enough, as is the case with the reball from previous tests, both upchirp and downchirp beat frequencies from the moving target will appear on the same side of the frequency offset. This scenario, in the case that the reball is moving away from the radar system, can be seen in figure 6-2.

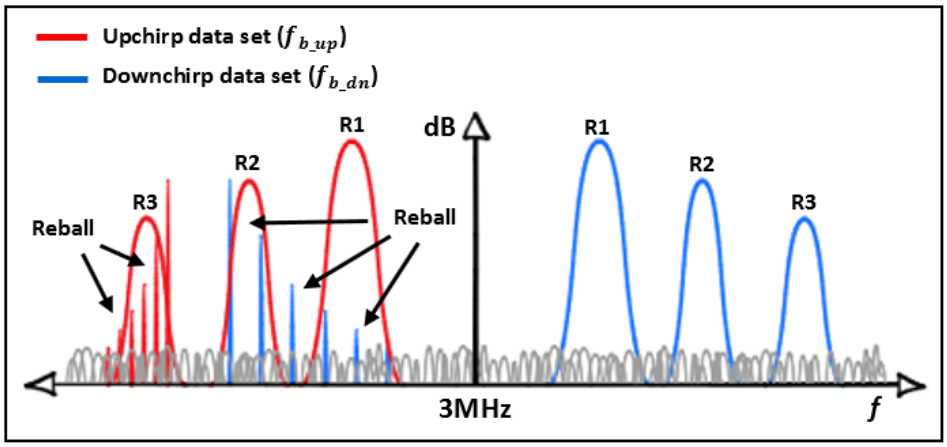

Figure 6-2: An illustration of the combined upchirp and downchirp return signals obtained over a short period of time when transmitting a triangular waveform with $\tau_{up} = \tau_{dn}$ and frequency offset $\Delta f_c = 3$ MHz. Three static targets at ranges R1, R2, & R3 are in the scene simultaneously with a high-velocity target (reball) that is moving away from the radar system. The echo signal from the reball is being obscured by the echo signal from static targets.

It appears from figure 6-2 that both the upchirp and downchirp return signals from the reball are being obscured by static clutter from the stationary targets. But if the signal data from figure 6-2 were separated based on whether it was collected during an upchirp or a downchirp, it would be apparent that only the moving target downchirp beat frequency is being obscured, as shown in figure 6-3.

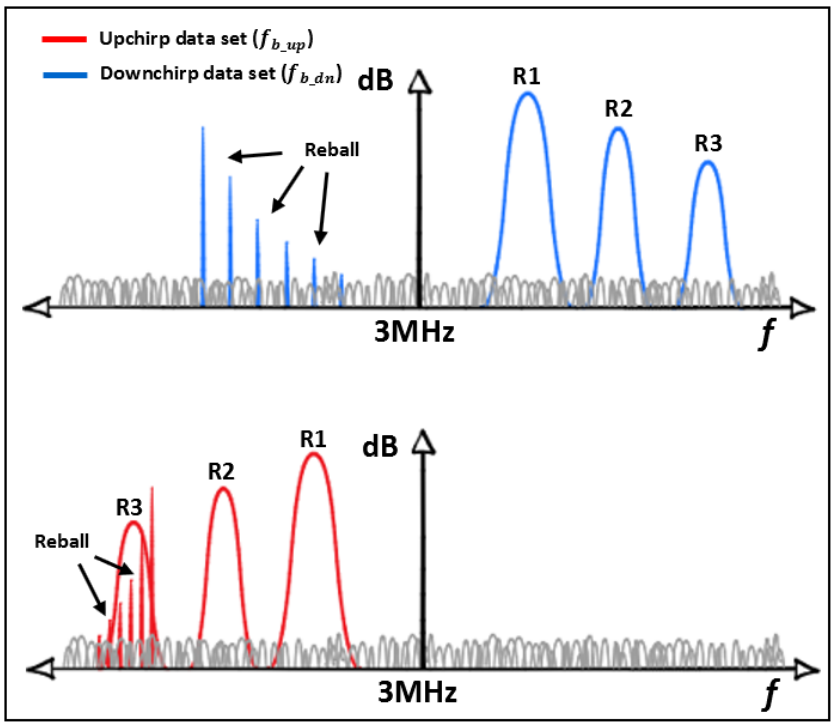

Figure 6-3: Upchirp and downchirp beat frequency data after being parsed into two different data sets. The reball's downchirp beat frequency signals are isolated from the static clutter, but its upchirp beat frequency signals are still obscured.

We can see from figure 6-3 that after parsing the received data into the upchirp and downchirp data sets, the reball return signal within the downchirp data set is already spectrally isolated from the static clutter. However, the reball signal from the upchirp data set is still being obscured. In this scenario, the downchirp data set alone is sufficient to detect the reball. But, as previously discussed, before range and velocity can be determined, the reball return signal from both data sets needs to be recovered.

Knowing that all static clutter from the downchirp data set is mirrored in the upchirp data set, we can use the downchirp data above the 3 MHz offset to suppress the static clutter in the upchirp data set and improve the reball detectability. The steps needed to achieve this are shown visually in figure 6-4 below.

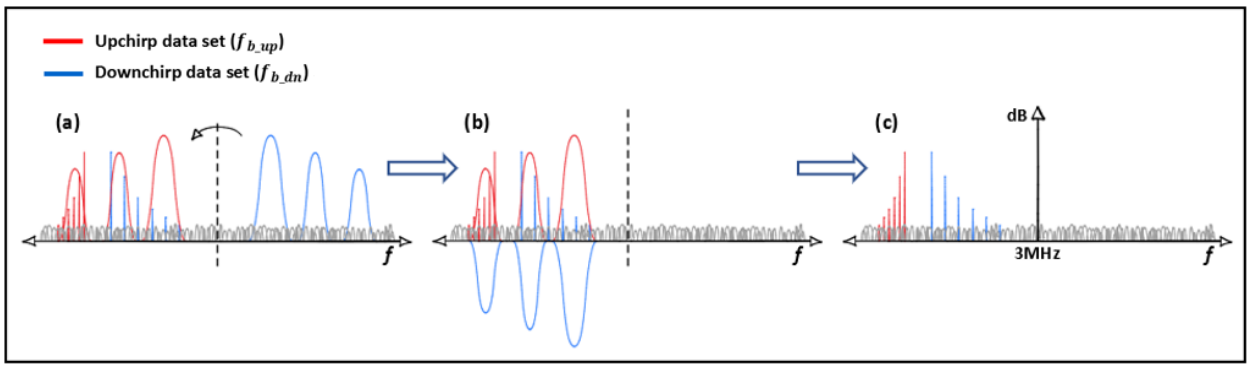

Figure 6-4: (a) Downchirp data above frequency offset is folded over the frequency offset. (b) The portion of the downchirp data vector that was folded over is then inverted. (c) Both data sets are added together, causing static clutter to cancel.

To explain the method depicted in figure 6-4 more mathematically, the process by which static clutter can be effectively suppressed without significantly affecting the reball signal is as follows. First, for each downchirp, define a vector containing the complex voltage values that lie above the frequency offset.

$$\chi_{dn}(f) = V_{dn}(f)e^{-j\varphi_{dn}(f)} \quad \text{for} \quad (\Delta f_c < f \leq f_{max}) \tag{6.1}$$

Where $V_{dn}(f)$ and $\varphi_{dn}(f)$ are the magnitude and phase of the complex voltage at frequency f for the downchirp data set.

Likewise, for each subsequent upchirp, define a vector containing the complex voltage values that lie below the frequency offset.

$$\chi_{up}(f) = V_{up}(f)e^{-j\varphi_{up}(f)} \quad \text{for} \quad (f_{min} \leq f < \Delta f_c) \tag{6.2}$$

Where $V_{up}(f)$ and $\varphi_{up}(f)$ are the magnitude and phase of the complex voltage at frequency f for the upchirp data set. For equations (6.1) and (6.2), f_{max} and f_{min} are pre-determined upper and lower frequency bounds, selected such that any possible beat frequencies of interest will be in the domain of f. These bounds should also be chosen so that the vector lengths of $\chi_{up}(f)$ and $\chi_{dn}(f)$ are equivalent. In other words, $|\Delta f_c - f_{max}| = |\Delta f_c - f_{min}|$.

In the example illustrated in figure 6-4, it is the static clutter from the upchirp data set that needs to be suppressed. This will typically be the case when the high-velocity target is moving away from the radar system and therefore has a large negative Doppler shift. To suppress the clutter in the upchirp data set, the clutter from the downchirp data set will be used. These clutter signals are contained in the vector $\chi_{dn}(f)$, defined in equation (6.1). However, the order of the elements in $\chi_{dn}(f)$ need to be reversed so that the clutter signals contained in it will line up with the corresponding clutter signals in $\chi_{up}(f)$.

$$\chi_{dn}([f],[f+1]\ldots[f_{max}]) \rightarrow \chi_{dn\_rev}([f_{max}],[f_{max}-1]\ldots[f]) \qquad (6.3)$$

For best results, both upchirp and downchirp vectors need to have identical (but conjugate) phase information, so that $\varphi_{dn}(f) = -\varphi_{up}(f)$. Therefore, the phase of each element of $\chi_{dn\_rev}(f)$ was removed and replaced with the conjugate of the phase of the corresponding element from $\chi_{up}(f)$. This results in a new complex vector that can be used to suppress static clutter in the upchirp data set. The upchirp clutter suppression vector $\chi_{cs\_up}(f)$ is defined as:

$$\chi_{cs\_up}(f) = |\chi_{dn\_rev}(f)|e^{+j\varphi_{up}(f)} \quad \text{for} \quad (f_{min} \leq f < \Delta f_c) \qquad (6.4)$$

Now that the upchirp and downchirp data vectors are properly aligned and each pair of corresponding elements has conjugate phase information, the clutter suppression vector can be subtracted from the upchirp data vector, element by element.

$$\chi'_{up}(f) = \chi_{up}(f) - \chi_{cs\_up}(f) \quad \text{for} \quad (f_{min} \leq f < \Delta f_c) \qquad (6.5)$$

Where $\chi'_{up}(f)$ is the upchirp data vector after static clutter has been suppressed.

By following these steps, the only signal data that should be suppressed will be those that meet the condition that $\chi_{up}(f) = -\chi_{dn}(f)$, which can only be true for objects whose relative

radial velocity is equal to zero. The results of applying this method of static clutter suppression on actual data can be seen below.

Figure 6-5 contains two plots showing 100 ms of beat frequency data after it has been parsed into separate upchirp and downchirp data sets, before enabling clutter suppression. The reball was fired away from the radar and is detectable for approximately 50 ms of flight time.

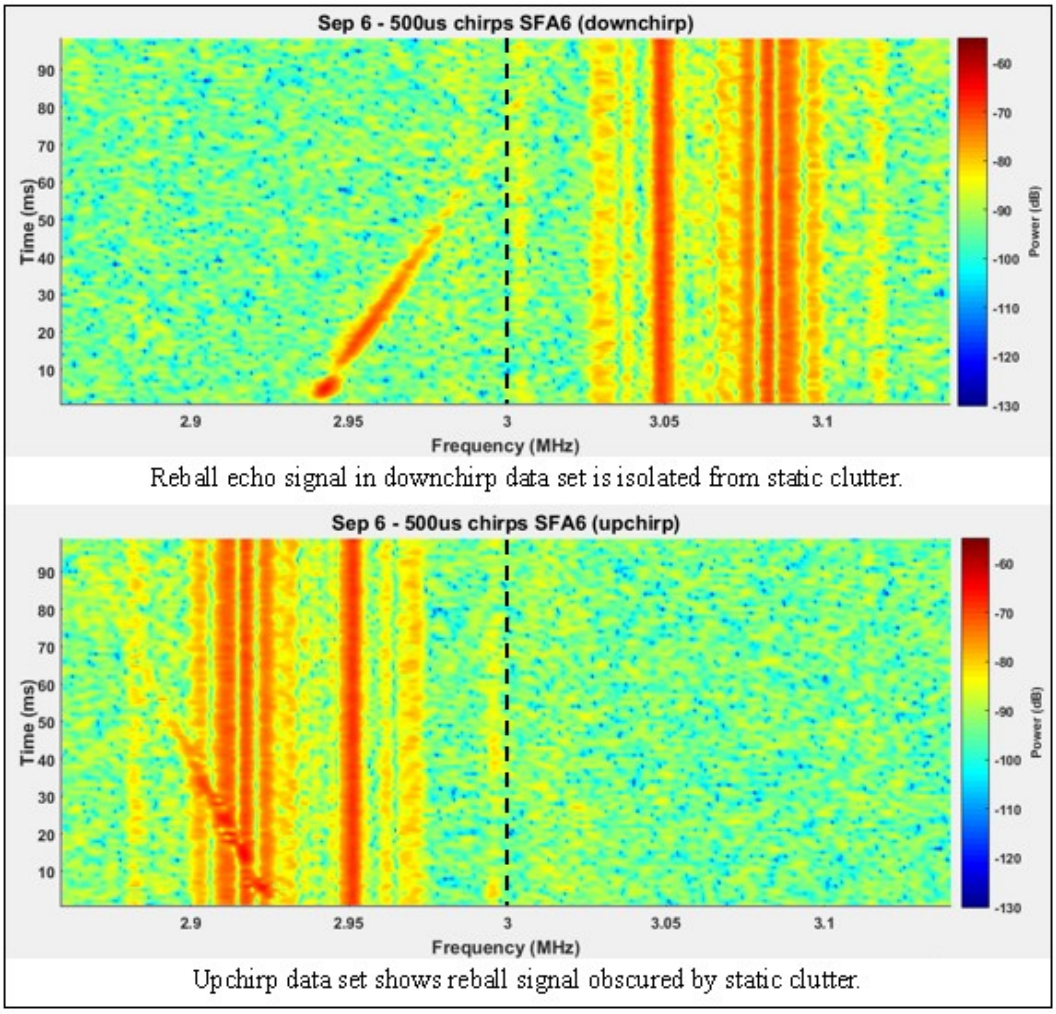

Figure 6-5: Reball echo signal data recorded over 100 ms in a clutter-heavy environment. Upchirp and downchirp durations are both 0.5 ms so that, for stationary targets, $f_{b\_up} = -f_{b\_dn}$. Because of the large negative Doppler frequency shift due to the reball travelling away from the radar, the reball's return signal appears below 3 MHz in both data sets.

In the downchirp data set, because the reball is travelling away from the radar system, its negative Doppler shift separates the reball signal from the static clutter which has a positive beat frequency. In the upchirp data set, both the reball and the static clutter have comparable negative beat frequencies, resulting in the reball signal being obscured by the static clutter. Applying a peak detection algorithm to the upchirp data set reveals how the clutter makes it more difficult to accurately determine range and velocity. The results of calculating range and velocity based on the upchirp and downchirp data prior to clutter suppression can be seen in the following figure.

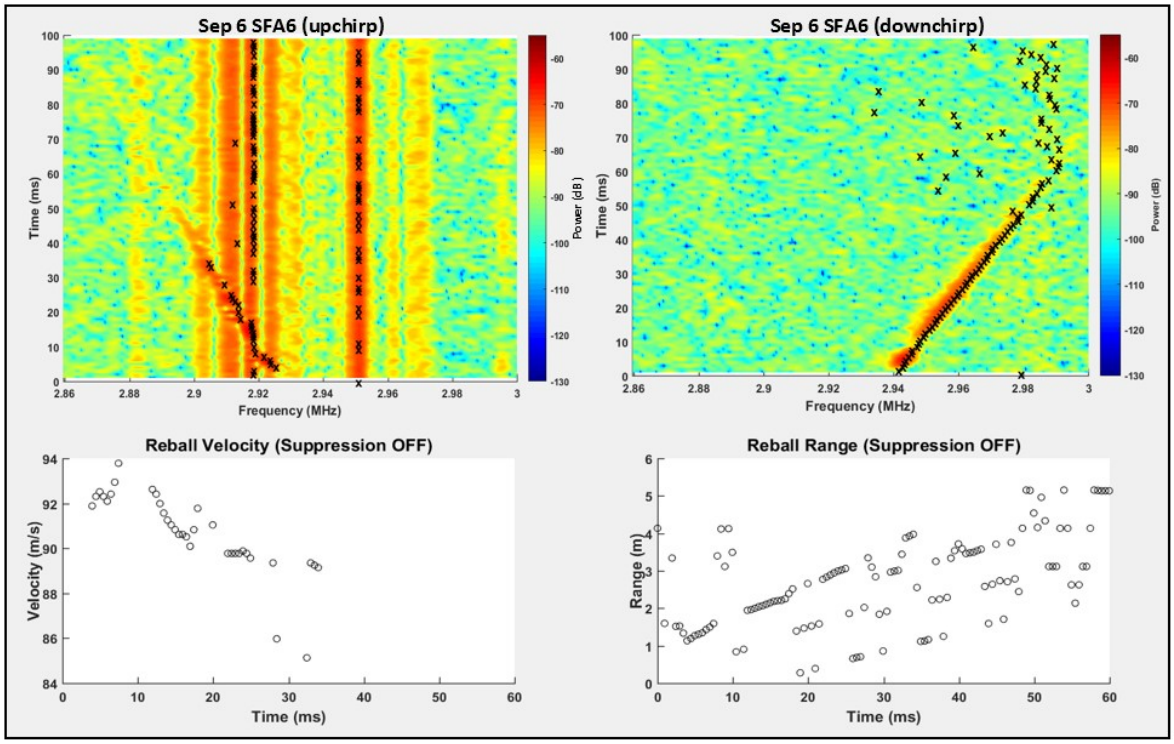

Figure 6-6: Upchirp and downchirp data sets with no clutter suppression enabled. A peak detection algorithm is used in MATLAB to select the strongest return signal for each 0.5 ms upchirp and downchirp. These are marked with X's in the top two plots. The bottom two plots show the point-by-point range and velocity calculations for the marked points, using equations (5.10) & (5.16).

As shown in figure 6-6, the range and velocity information are unreliable in this case because the interference from the clutter compromised the ability to consistently track the reball signal. After enabling clutter suppression, the static clutter in the upchirp data set is greatly

attenuated, and the ability to calculate range and velocity is substantially increased, as can be seen in figure 6-7 below.

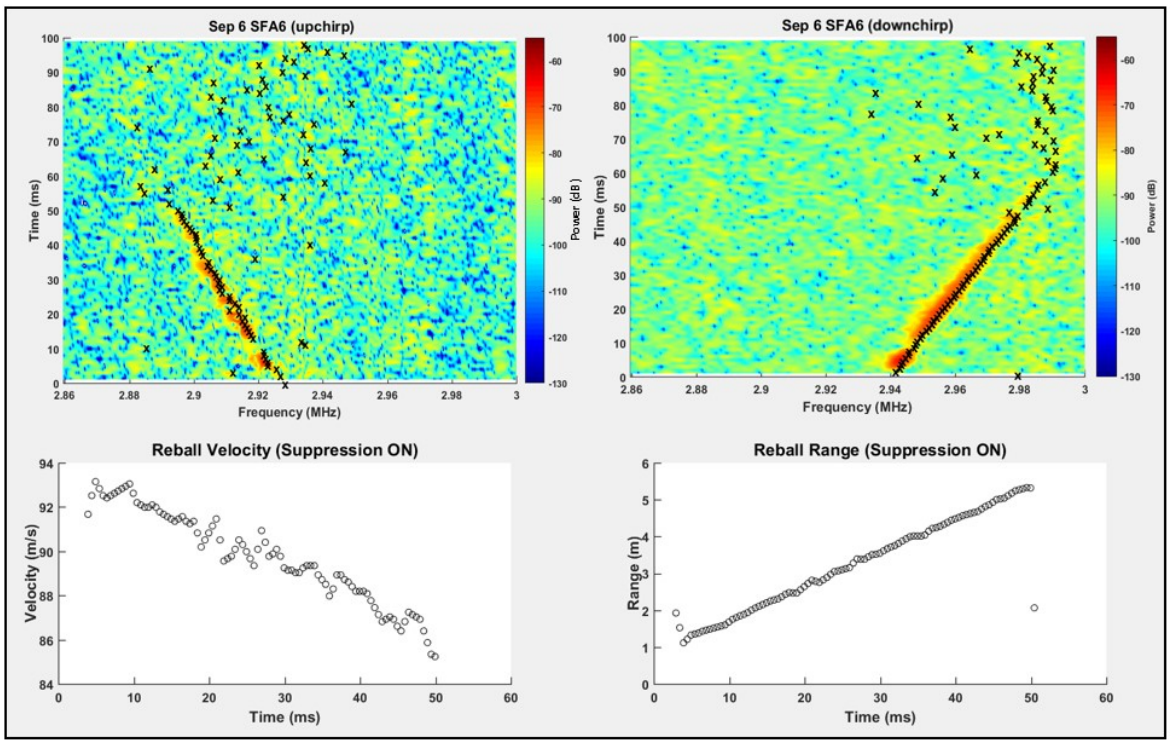

Figure 6-7: Reball signal from upchirp and downchirp data sets after enabling clutter suppression. Ability to measure range and velocity is significantly improved when compared to results from figure 6-6.

While the clutter signals in this test were suppressed by upwards of 20 dB, making the reball more easily detectable, the reball signal is also affected by the suppression process. This is most likely because the upchirp data vectors that were used to cancel the downchirp clutter also contained the complex voltage values of the noise at each point in the observed frequency range. As a result, the reball SNR dropped by about 3 dB, and the reball's overall signal quality was slightly degraded, leading to the non-linearities seen in the bottom left plot of figure 6-7. However, the resulting data is enough to show that for this shot, the reball had an initial velocity of about 94 m/s, deceleration of 0.16 m/s/ms, and that it was detectable at a range of up to about 5.3 meters.

The range and velocity plots in figures 6-6 and 6-7 were derived from equations (5.10) and (5.16), both of which only take into account the current upchirp or downchirp and its two neighboring chirps. As previously discussed, this method simulates the degree of accuracy that could be expected if range and velocity were being determined in real time.

More accurate results can be obtained during post-processing if the entire beat frequency vector is analyzed together. By doing so, a first order equation can be derived using MATLAB or Microsoft Excel to express the reballs upchirp and downchirp beat frequencies as functions of time. Equation (5.17) can then be used to derive a function for reball Doppler frequency, as shown in figure 6-8 below.

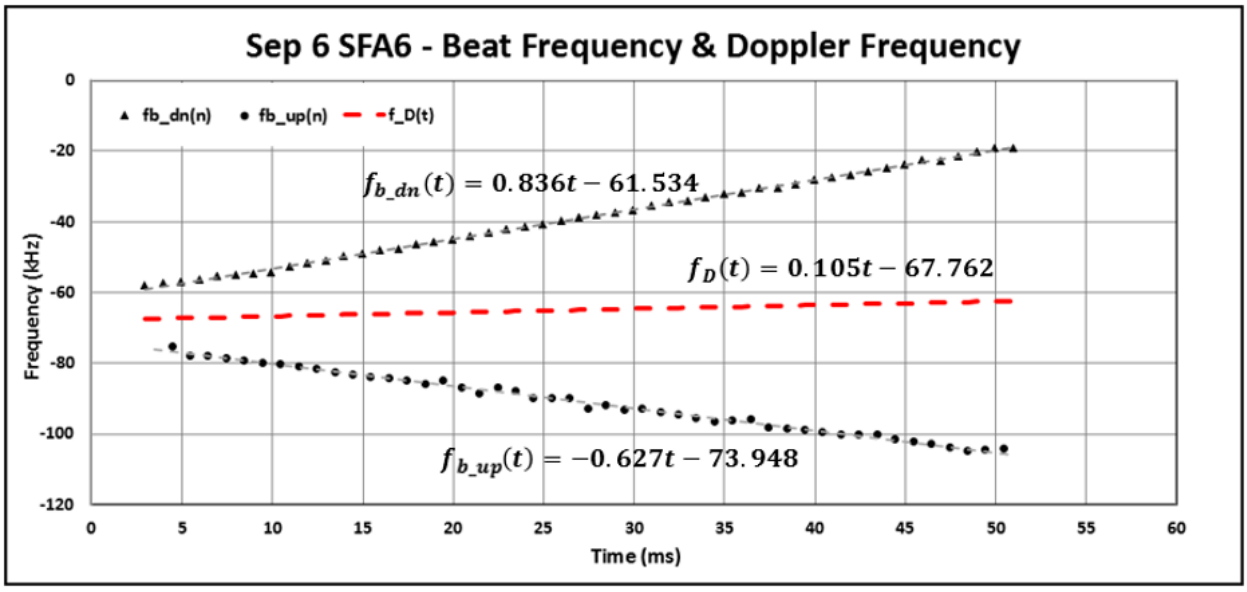

Figure 6-8: Reball beat frequency and Doppler frequency expressed as functions of time.

At this point, the functions $f_{b\_up}(t)$, $f_{b\_dn}(t)$, and $f_D(t)$ can be inserted into equations (5.18) and (5.23) to determine functions for both range and velocity. If functions $R(t)$ and $v(t)$ are plotted over the same time duration that the reball was detected, these functions can be

compared to the initial results seen in the range and velocity plots from figure 6-7. This is done in figure 6-9 below.

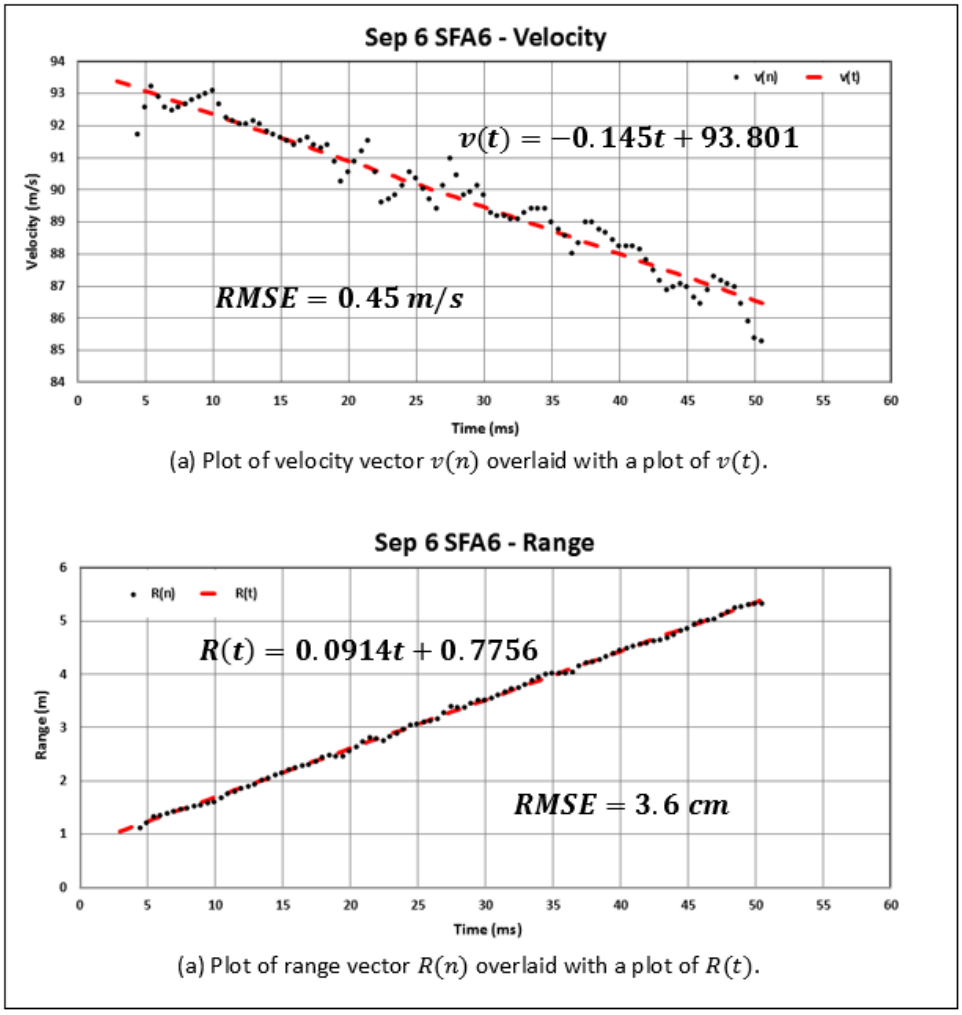

Figure 6-9: A comparison between obtaining each range and velocity measurement using three subsequent beat frequency samples, as described in figure 5-4, versus deriving range and velocity functions from the beat frequency and Doppler frequency functions seen in figure 6-8. The vectors v(n) and R(n) can be obtained in real time, while the functions R(t) and v(t) are obtained in post-processing.

Figure 6-9 illustrates how the derived range and velocity functions give a better approximation of the actual range and velocity for a moving target. This is especially true when the moving target signal is not fully recoverable, or if the signal quality was degraded during the clutter suppression process, as was the case for this test.

Chapter 7. Conclusion

A dual-purpose W-Band radar system was configured to operate in FMCW mode, transmitting a triangular waveform. DDS trigger signals were recorded, along with target echo signals, so that echo signals that occurred during upchirps could be separated from those that occurred during downchirps, allowing for the creation of two data sets. Stretch Processing was implemented, and FFTs performed on each data set. When the upchirp duration and downchirp duration of the triangular waveform were equivalent, the beat frequencies of stationary targets were shown to be equal and opposite in magnitude in both data sets ($f_{b\_up} = -f_{b\_dn}$), while the beat frequencies of moving targets were not.

A frequency offset of 3 MHz was introduced between the transmit signal and the reference signal, so that when Stretch Processing was performed, the resulting target beat frequencies would be centered around 3 MHz instead of DC. This made it easier to distinguish between positive and negative Doppler, and made it possible to determine which data set contained upchirp signal data, and which contained downchirp signal data. The frequency offset also enabled clutter suppression to be performed by taking the static clutter return signals from one data set, reflecting them across the frequency offset, and subtracting them from the other data set. Using this method, static clutter suppression of up to 25 dB was achieved, while moving target signals suffered only a 3 dB loss in SNR.

The moving target of interest for tests performed was a reusable paintball (reball). Reball range and velocity were accurately measured at distances up to 5 meters and at speeds ranging

from 84 – 109 m/s (188 - 244 mph) with decelerations of approximately 0.155 m/s/ms (meters per second per millisecond).

Future work for this project might include investigation of signal phase continuity when alternating between upchirps and downchirps using a DDS. If there is phase discontinuity between chirps, it could explain why using phase information from both upchirp and downchirp data sets had undesirable results, while copying phase values from one data set to the other data set greatly improved clutter suppression.

Improvements could also be made in the frequency granularity of the return signals when FFTs are performed. Once the data enters the digital domain, a finite number of elements are used to describe a continuous frequency spectrum. This was a problem when trying to obtain two data vectors that were symmetric about the 3 MHz offset for clutter suppression. If one of the elements in the discrete frequency spectrum were exactly 3 MHz, or if the two elements above and below 3 MHz were equidistant from 3 MHz, the clutter signals contained in the upchirp and downchirp vectors would line up better, element by element, and clutter suppression would be even more effective. Achieving perfectly symmetric data vectors is unlikely, but it could be improved by increasing the sampling rate, or by further zero-padding the FFT.

Other future work could be to implement the described waveforms, frequency offset, and clutter suppression methods on a radar system with multiple receive antennas, so that stationary and moving targets could be mapped in elevation and azimuth, in addition to mapping range. This would also make it possible to determine the direction of moving targets. Other waveforms, which the current DDSs were unable to produce, could also be experimented with. These might include sawtooth waveforms with alternating chirp durations or non-linear waveforms.

References

[1] E. Hyun, W. Oh and J.-H. Lee, "Two-Step Moving Target Detection Algorithm for Automotive 77 GHz FMCW Radar," *IEEE Vehicular Tech. Conference Fall (VTC)*, pp. 1-5, Sept. 2010

[2] E. Hyun, W. Oh and J.-H. Lee, "Detection and Tracking Algorithm for 77GHz Automotive FMCW Radar," *2011 3rd International APSAR*, pp. 1-3, Nov. 2011

[3] H. Rohling and M. Kronauge, "New Radar Waveform based on a Chirp Sequence," *2014 International Radar Conference*, Lille, France, pp. 1-4, Oct. 2014

[4] L. Shi, C. Allen, M. Ewing, S. Keshmiri, M. Zakharov, F. Florencio, N. Niakan and R. Knight, "Multichannel Sense-and-Avoid Radar for Small UAVs," *2013 IEEE/AIAA 32nd DASC*, pp. 1-10, Oct. 2013

[5] C. R. Nave. "Hyperphysics." http://hyperphysics.phy-astr.gsu.edu/hbase/Sound/beat.html (accessed July 15, 2019)

APPENDIX A

Radar System & Test setup:

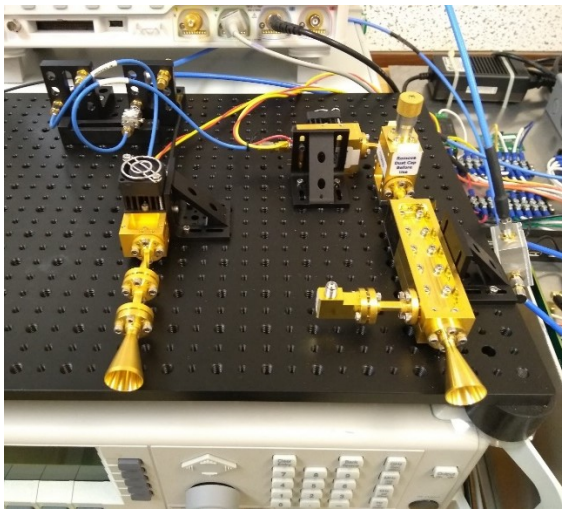

Rx antenna (left) & Tx antenna (right)

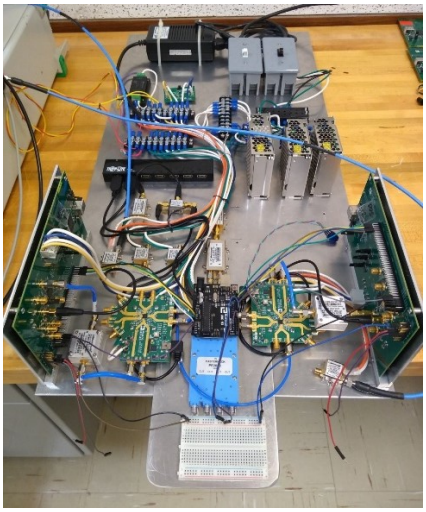

Aluminum plate with mounted components

Shot fired away from radar system (SFA)

Shot fired towards radar system (behind sheet)

Ripple in sheet increases sheet's RCS

Additional test results for shots fired towards and away from radar system:

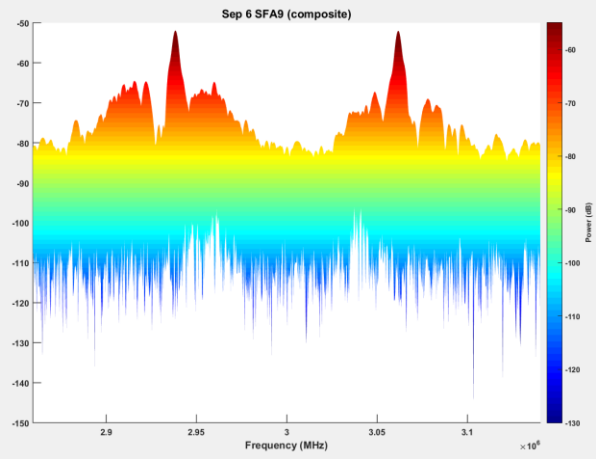

Composite signal spectrum before suppression

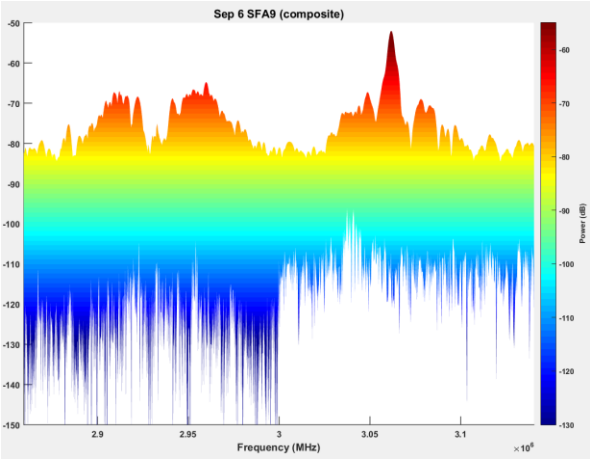

Composite signal spectrum after suppression

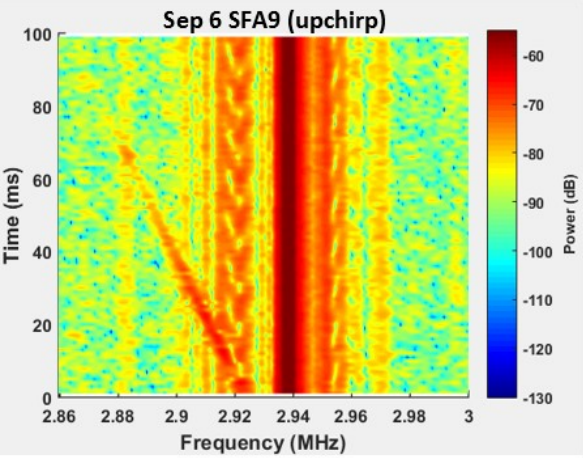

Upchirp surface plot before suppression (SFA)

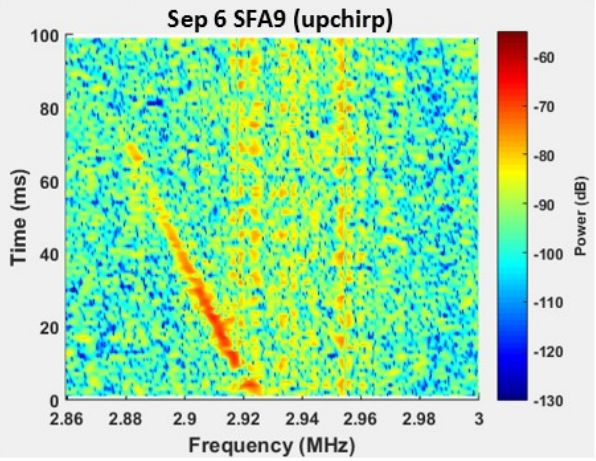

Upchirp surface plot after suppression (SFA)

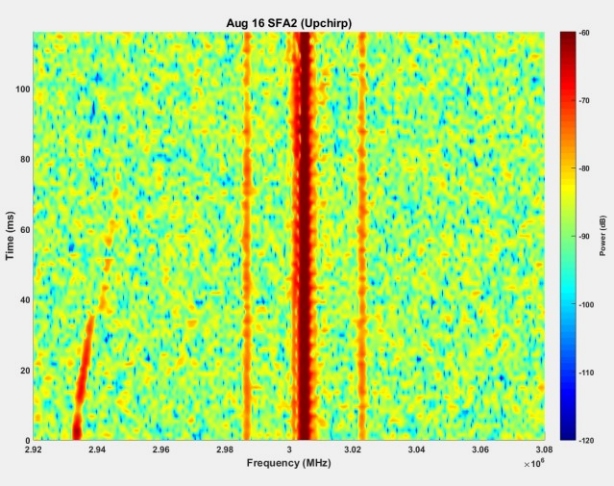

Surface plot of 3 ms downchirp data set (SFA):

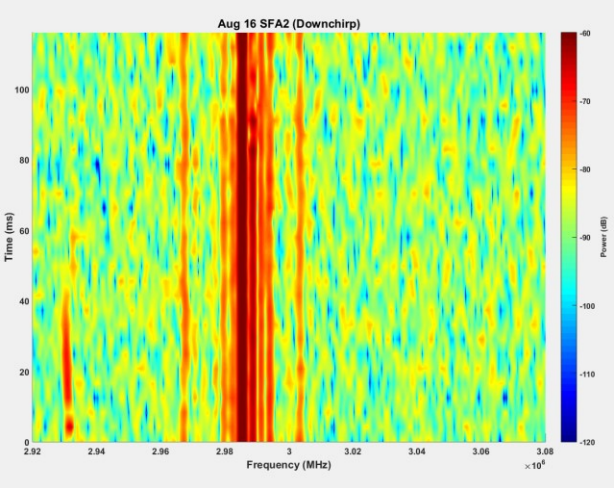

Surface plot of 1 ms upchirp data set (SFA):

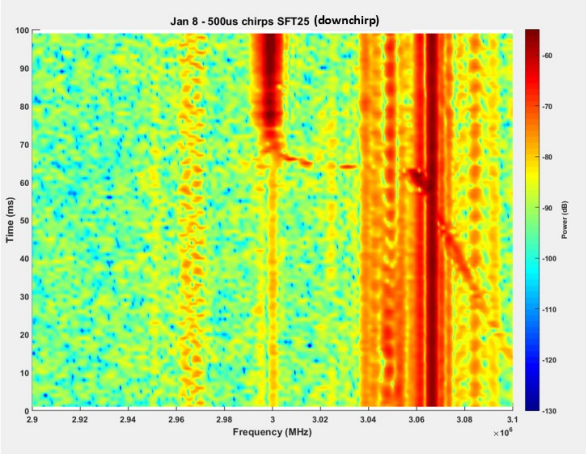

Downchirp data set before suppression (SFT)

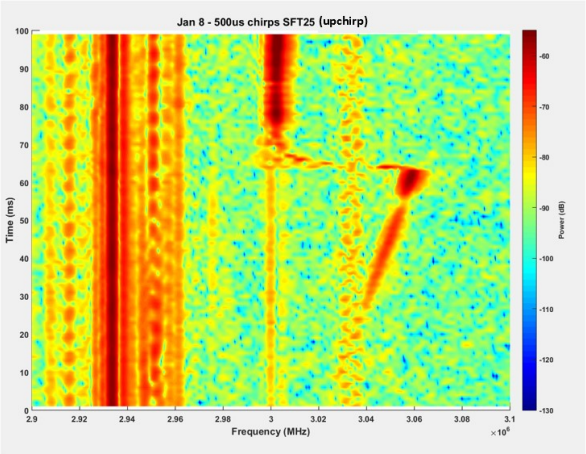

Upchirp data set (SFT)

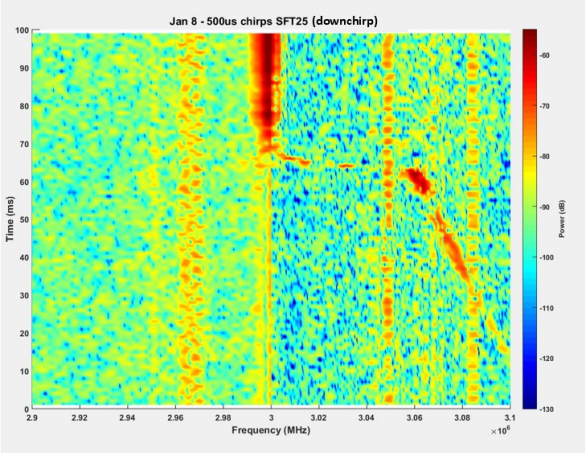

Downchirp data set after suppression (SFT). Return signal from sheet appears stronger after contact because ripple in sheet increases it's RCS.

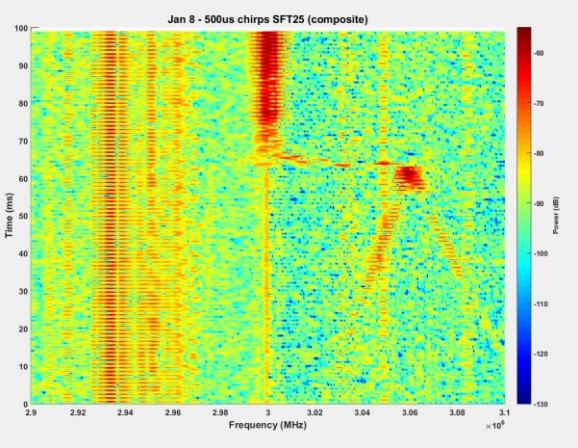

Composite upchirp and downchirp data sets. Reball beat frequencies converge as reball range approaches zero. At this point, upchirp and downchirp beat frequencies are equivalent.

Reball RCS calibration test results:

Given RCS for calibration targets:

6” Trihedral RCS @ 108 GHz: ~ 18.7 dBsm

4” Sphere RCS @ 108 GHz: ~ -20.9 dBsm

Expected RCS of conductive sphere with diameter of 0.6875 inches: ~ -36.2 dBsm

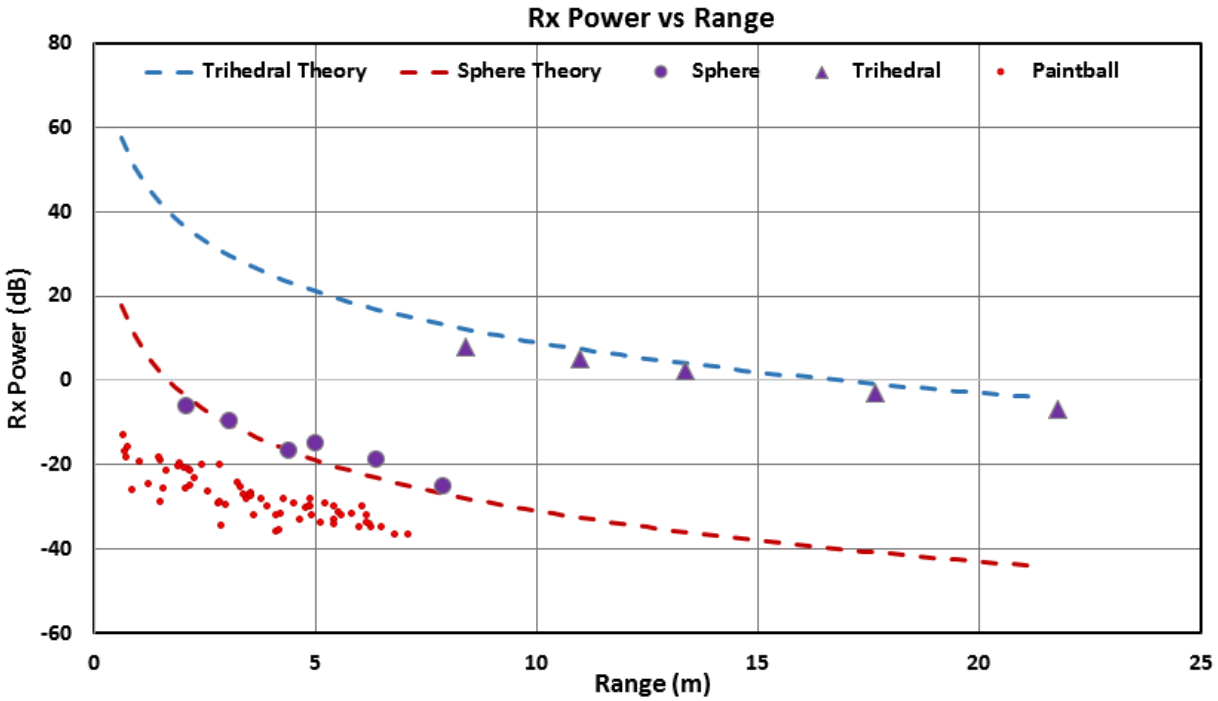

Reball return signal strength is approximately 52 dB lower than trihedral, and 12 dB lower than sphere. Therefore, measured reball RCS is ~ -33 dBsm at 108 GHz. This is in close agreement with theoretical RCS for sphere of diameter 0.6875 in.

APPENDIX B

System block diagram:

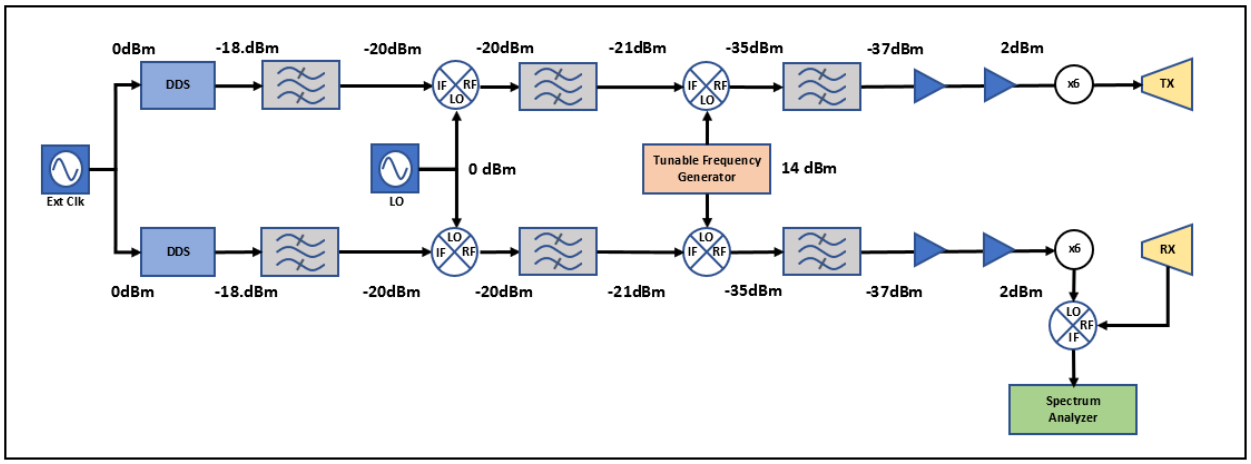

System block diagram with power levels at the input and output of each component:

Oscilloscope parameters and FFT lengths for 240 MHz and 600 MHz signal bandwidths:

	240 MHz			600 MHz
Sampling Rate	10 MSPS			20 MSPS
Record Time Duration	150 ms			100 ms
Sample points per 0.5 ms	5 k			10 k
Chirp Duration	1 ms	3 ms	15 ms	0.5 ms
FFT Length	2^{16}	2^{17}	2^{20}	65536-point (2^{16})

Relevant equations not found in text:

Range Resolution: $\Delta R = \frac{c}{2B}$ Range Accuracy: $\delta R \cong \frac{\Delta R}{\sqrt{2SNR}}$

Root Mean Squared Error: $RMSE = \sqrt{\frac{(a_1-b_1)^2+(a_2-b_2)^2+\cdots+(a_n-b_n)^2}{n}}$

Product of two signals: $\cos(\omega_1)\cos(\omega_2) = \frac{\cos(\omega_1+\omega_2)+\cos(\omega_1-\omega_2)}{2}$

APPENDIX C

Select Component Datasheets:

Data Sheet ADRF6780

SPECIFICATIONS

VPBB = VPBI = VPLO = 3.3 V, VP18 = 1.8 V, VPDT = VPRF = 5 V, T_A = 25°C, LO = 0 dBm differential drive; baseband I/Q amplitude = −15 dBm differential sine waves in quadrature with a 500 mV dc bias, baseband input termination with 100 Ω externally, IF amplitude = −12 dBm differential sine waves, unless otherwise noted.

Table 1.

Parameter	Test Conditions/Comments	Min	Typ	Max	Unit
RF OUTPUT FREQUENCY RANGE		5.9		23.6	GHz
LOCAL OSCILLATOR (LO) INPUT FREQUENCY RANGE		5.4		14	GHz
LO AMPLITUDE RANGE		−6	0	+6	dBm
IF INPUT FREQUENCY RANGE		0.8		3.5	GHz
BASEBAND (BB) I/Q INPUT FREQUENCY RANGE		DC		750	MHz
I/Q MODULATOR PERFORMANCE					
Modulator Voltage Gain	Maximum gain at maximum gain setting	10	13		dB
	Minimum gain at minimum gain setting		−12		dB
Output Noise Density	Output carrier > −5 dBm		−147		dBc/Hz
	Output carrier > −14 dBm		−145		dBc/Hz
	Output carrier > −22.5 dBm		−136		dBc/Hz
Output Third-Order Intercept (OIP3)	f_{1BB} = 10 MHz, f_{2BB} = 12 MHz, BB I/Q amplitude per tone = −15 dBm sine waves in quadrature with a 500 mV dc bias, 10 dB gain setting				
5.9 GHz to 10 GHz			24		dBm
10 GHz to 14 GHz			25		dBm
14 GHz to 20 GHz			27		dBm
20 GHz to 23.6 GHz			27		dBm
Fifth-Order Intermodulation Distortion (IMD5)	f_1 BB = 10 MHz, f_2 BB = 12 MHz, baseband I/Q amplitude per tone = −15 dBm sine waves in quadrature with a 500 mV dc bias, 10 dB gain setting		65		dBm
Output Second-Order Intercept (OIP2)	f_1 BB = 10 MHz, f_2 BB = 12 MHz, baseband I/Q amplitude per tone = −15 dBm sine waves in quadrature with a 500 mV dc bias, 10 dB gain setting				
5.9 GHz to 10 GHz			65		dBm
10 GHz to 14 GHz			65		dBm
14 GHz to 20 GHz			66		dBm
20 GHz to 23.6 GHz			50		dBm
Output 1 dB Compression Point (P1dB)					
5.9 GHz to 10 GHz	At 10 dB gain setting		10.5		dBm
	At maximum gain setting		11		dBm
10 GHz to 14 GHz	At 10 dB gain setting		11		dBm
	At maximum gain setting		12		dBm
14 GHz to 20 GHz	At 10 dB gain setting		10		dBm
	At maximum gain setting		12		dBm
20 GHz to 23.6 GHz	At 10 dB gain setting		10		dBm
	At maximum gain setting		11		dBm
LO Feedthrough	At 10 dB gain setting (can be improved baseband dc offset adjustment)		−25		dBm
Sideband Suppression	At 10 dB gain setting		25		dBc

Parameter	Test Conditions/Comments	Min	Typ	Max	Unit
IF UPCONVERTER PERFORMANCE					
Upconversion Voltage Gain	Maximum gain at maximum gain setting	7	11		dB
	Minimum gain at minimum gain setting		−14		dB
Output Noise Density	Output carrier > −5 dBm		−147		dBc/Hz
	Output carrier > −14 dBm		−145		dBc/Hz
	Output carrier > −22.5 dBm		−136		dBc/Hz
OIP3	f_1 IF = 1810 MHz, f_2 IF = 1812 MHz, amplitude per tone = −15 dBm sine waves in quadrature with ac bias, 7 dB gain setting		23.5		
5.9 GHz to 10 GHz			27		dBm
10 GHz to 14 GHz			24		dBm
14 GHz to 20 GHz			22.5		dBm
20 GHz to 23.6 GHz			22.5		dBm
IMD5	f_1 IF = 1810 MHz, f_2 IF = 1812 MHz, amplitude per tone = −15 dBm sine waves in quadrature with ac bias, 7 dB gain setting		80		dBm
Output P1dB					
5.9 GHz to 10 GHz	At 7 dB gain setting		10.5		dBm
	At maximum gain setting		11.5		dBm
10 GHz to 14 GHz	At 7 dB gain setting		10		dBm
	At maximum gain setting		12		dBm
14 GHz to 20 GHz	At 7 dB gain setting		9.5		dBm
	At maximum gain setting		12		dBm
20 GHz to 23.6 GHz	At 7 dB gain setting		9.5		dBm
	At maximum gain setting		11.5		dBm
LO Feedthrough	At 7 dB gain setting (can be improved by baseband dc offset adjustment)		−35		dBm
Sideband Suppression	At 7 dB gain setting		25		dBc
Tx POWER DETECTOR PERFORMANCE					
Output Level					
Maximum			2		dBm
Minimum			−30		dBm
±1 dB Dynamic Range			34		dB
Output Voltage					
Maximum			1		V
Minimum			0.2		V
Log Slope			25		mV/dB
Time					
Rise	P_{IN} = off to −10 dBm, 10% to 90%, C7 = 10 pF (see Figure 83)		134		ns
Fall	P_{IN} = −10 dBm to off, 10% to 90%, C7 = 10 pF (see Figure 83)		190		ns
Response	C7 = 10 pF (see Figure 83)		30		ns
RETURN LOSS					
RF Output	100 Ω differential		12		dB
LO Input	100 Ω differential		12		dB
IF Input	100 Ω differential		17		dB
Baseband I/Q Input Impedance			1		MΩ
LOGIC INPUTS					
Input High Voltage Range, V_{INH}		VP18 − 0.4		1.8	V
Input Low Voltage Range, V_{INL}		0		0.4	V
Input Current, I_{INH}/I_{INL}			100		µA
Input Capacitance, C_{IN}			3		pF

Parameter	Test Conditions/Comments	Min	Typ	Max	Unit
LOGIC OUTPUTS					
Output High Voltage Range, V_{OH}		VP18 – 0.4		1.8	V
Output Low Voltage Range, V_{OL}		0		0.4	V
Output High Current, I_{OH}				500	µA
POWER INTERFACE					
VPBB, VPLO, VPBI		3.15	3.3	3.45	V
VPBB, VPLO, VPBI Supply Current	×1 LO path enabled, IF path disabled		340		mA
	×2 LO path enabled, IF path disabled		390		mA
	×1 LO path enabled, IF path enabled		490		mA
	×2 LO path enabled, IF path enabled		540		mA
VP18		1.7	1.8	1.9	V
VP18 Supply Current			1		mA
VPDT, VPRF		4.75	5	5.25	V
VPDT, VPRF Supply Current	×1/×2 LO path enabled, IF path disabled		180		mA
	×1/×2 LO path enabled, IF path enabled		160		mA
Total Power Consumption	×2 LO path enabled, IF path enabled		2.58		W
	Power down		35	50	mW

ABSOLUTE MAXIMUM RATINGS

Table 2.

Parameter	Rating
Supply Voltage	
VPDT, VPRF	6.5 V
VPBB, VPLO, VPBI	4.3 V
VP18	2.3 V
Maximum Junction Temperature	150°C
Operating Temperature Range	−40°C to +85°C
Storage Temperature Range	−55°C to +125°C
Lead Temperature Range (Soldering 60 sec)	−65°C to +150°C

Stresses at or above those listed under Absolute Maximum Ratings may cause permanent damage to the product. This is a stress rating only; functional operation of the product at these or any other conditions above those indicated in the operational section of this specification is not implied. Operation beyond the maximum operating conditions for extended periods may affect product reliability.

THERMAL RESISTANCE

θ_{JA} is thermal resistance, junction to ambient (°C/W), and θ_{JC} is thermal resistance, junction to case (°C/W).

Table 3. Thermal Resistance

Package Type	θ_{JA}[1]	θ_{JC}[1]	Unit
32-Lead LFCSP	32.95	1.14	°C/W

[1] See JEDEC standard JESD51-2 for additional information on optimizing the thermal impedance (printed circuit board (PCB) with 3 × 3 vias).

ESD CAUTION

ESD (electrostatic discharge) sensitive device. Charged devices and circuit boards can discharge without detection. Although this product features patented or proprietary protection circuitry, damage may occur on devices subjected to high energy ESD. Therefore, proper ESD precautions should be taken to avoid performance degradation or loss of functionality.

SPECIFICATIONS

DC SPECIFICATIONS

AVDD (1.8 V) and DVDD (1.8 V) = 1.8 V ± 5%, AVDD (3.3 V) and DVDD_I/O (3.3 V) = 3.3 V ± 5%, T_A = 25°C, R_{SET} = 3.3 kΩ, I_{OUT} = 20 mA, external reference clock frequency = 2.5 GHz with reference clock (REF CLK) multiplier bypassed, unless otherwise noted.

Table 1.

Parameter	Min	Typ	Max	Unit	Test Conditions/Comments
SUPPLY VOLTAGE					
DVDD_I/O	3.135	3.30	3.465	V	Pin 16, Pin 83
DVDD	1.71	1.80	1.89	V	Pin 6, Pin 23, Pin 73
AVDD (3.3 V)	3.135	3.30	3.465	V	Pin 34, Pin 36, Pin 39, Pin 40, Pin 43, Pin 47, Pin 50, Pin 52, Pin 53, Pin 60
AVDD (1.8 V)	1.71	1.80	1.89	V	Pin 32, Pin 56, Pin 57
SUPPLY CURRENT					See also the total power dissipation specifications
$I_{DVDD\_I/O}$			20	mA	Pin 16, Pin 83
I_{DVDD}			270	mA	Pin 6, Pin 23, Pin 73
$I_{AVDD(3.3V)}$			640	mA	Pin 34, Pin 36, Pin 39, Pin 40, Pin 43, Pin 47, Pin 50, Pin 52, Pin 53, Pin 60
$I_{AVDD(1.8V)}$			148	mA	Pin 32, Pin 56, Pin 57
TOTAL POWER DISSIPATION					
Base DDS Power, PLL Disabled		2138	2797	mW	2.5 GHz, single-tone mode, modules disabled, linear sweep disabled, amplitude scaler disabled
Base DDS Power, PLL Enabled		2237	2890	mW	2.5 GHz, single-tone mode, modules disabled, linear sweep disabled, amplitude scaler disabled
Linear Sweep Additional Power		28		mW	
Modulus Additional Power		20		mW	
Amplitude Scaler Additional Power		138		mW	Manual or automatic
Full Power-Down Mode		400	616	mW	Using either the power-down and enable register or the EXT_PWR_DWN pin
CMOS LOGIC INPUTS					
Input High Voltage (V_{IH})	2.0		DVDD_I/O	V	
Input Low Voltage (V_{IL})			0.8	V	
Input Current (I_{INH}, I_{INL})		±60	±200	µA	At V_{IN} = 0 V and V_{IN} = DVDD_I/O
Maximum Input Capacitance (C_{IN})		3		pF	
CMOS LOGIC OUTPUTS					
Output High Voltage (V_{OH})	2.7		DVDD_I/O	V	I_{OH} = 1 mA
Output Low Voltage (V_{OL})			0.4	V	I_{OL} = 1 mA
REF CLK INPUT CHARACTERISTICS					REF CLK inputs must always be ac-coupled (both single-ended and differential)
REF CLK Multiplier Bypassed					
Input Capacitance		1		pF	Single-ended, each pin
Input Resistance		1.4		kΩ	Differential
Internally Generated DC Bias Voltage		2		V	
Differential Input Voltage		0.8	1.5	V p-p	
REF CLK Multiplier Enabled					
Input Capacitance		1		pF	Single-ended, each pin
Input Resistance		1.4		kΩ	Differential
Internally Generated DC Bias Voltage		2		V	
Differential Input Voltage		0.8	1.5	V p-p	

AC SPECIFICATIONS

AVDD (1.8 V) and DVDD (1.8 V) = 1.8 V ± 5%, AVDD3 (3.3 V) and DVDD_I/O (3.3 V) = 3.3 V ± 5%, T_A = 25°C, R_{SET} = 3.3 kΩ, I_{OUT} = 20 mA, external reference clock frequency = 2.5 GHz with reference clock (REF CLK) multiplier bypassed, unless otherwise noted.

Table 2.

Parameter	Min	Typ	Max	Unit	Test Conditions/Comments
REF CLK INPUT					Input frequency range
REF CLK Multiplier Bypassed					
Input Frequency Range	500		2500	MHz	Maximum f_{OUT} is 0.4 × f_{SYSCLK}
Duty Cycle	45		55	%	
Minimum Differential Input Level	632			mV p-p	Equivalent to 316 mV swing on each leg
System Clock (SYSCLK) PLL Enabled					
VCO Frequency Range	2400		2500	MHz	
VCO Gain (K_V)		60		MHz/V	
Maximum PFD Rate			125	MHz	
CLOCK DRIVERS					
SYNC_CLK Output Driver					
Frequency Range			156	MHz	
Duty Cycle	45	50	55	%	
Rise Time/Fall Time (20% to 80%)		650		ps	
SYNC_OUT Output Driver					10 pF load
Frequency Range			6.5	MHz	
Duty Cycle	33		66	%	CFR2 register, Bit 9 = 1
Rise Time (20% to 80%)		1350		ps	10 pF load
Fall Time (20% to 80%)		1670		ps	10 pF load
DAC OUTPUT CHARACTERISTICS					
Output Frequency Range (1st Nyquist Zone)	0		1250	MHz	
Output Resistance		50		Ω	Single-ended (each pin internally terminated to AVDD (3.3 V))
Output Capacitance		1		pF	
Full-Scale Output Current			20.48	mA	Range depends on DAC R_{SET} resistor
Gain Error	−10		+10	% FS	
Output Offset			0.6	µA	
Voltage Compliance Range	AVDD − 0.50		AVDD + 0.50	V	
Wideband SFDR					See the Typical Performance Characteristics section
122.5 MHz Output		−67		dBc	0 MHz to 1250 MHz
305.3 MHz Output		−66		dBc	0 MHz to 1250 MHz
497.5 MHz Output		−59		dBc	0 MHz to 1250 MHz
978.2 MHz Output		−60		dBc	0 MHz to 1250 MHz
Narrow-Band SFDR					See the Typical Performance Characteristics section
122.5 MHz Output		−95		dBc	±500 kHz
305.3 MHz Output		−95		dBc	±500 kHz
497.5 MHz Output		−95		dBc	±500 kHz
978.2 MHz Output		−92		dBc	±500 kHz
DIGITAL TIMING SPECIFICATIONS					
Time Required to Enter Power-Down		45		ns	Power-down mode loses DAC/PLL calibration settings
Time Required to Leave Power-Down		250		ns	Must recalibrate DAC/PLL
Minimum Master Reset time	24			SYSCLK cycles	
Maximum DAC Calibration Time (t_{CAL})			188	µs	See the DAC Calibration Output section for formula; Bit 6 in Register 0x1B = 0
Maximum PLL Calibration Time (t_{REF_CLK})			16	ms	PFD rate = 25 MHz
			8	ms	PFD rate = 50 MHz
Maximum Profile Toggle Rate			2	SYNC_CLK period	

ABSOLUTE MAXIMUM RATINGS

Table 3.

Parameter	Rating
AVDD (1.8 V), DVDD (1.8 V) Supplies	2 V
AVDD (3.3 V), DVDD_I/O (3.3 V) Supplies	4 V
Digital Input Voltage	−0.7 V to +4 V
Digital Output Current	5 mA
Storage Temperature Range	−65°C to +150°C
Operating Temperature Range	−40°C to +85°C
Maximum Junction Temperature	150°C
Lead Temperature (10 sec Soldering)	300°C

Stresses at or above those listed under Absolute Maximum Ratings may cause permanent damage to the product. This is a stress rating only; functional operation of the product at these or any other conditions above those indicated in the operational section of this specification is not implied. Operation beyond the maximum operating conditions for extended periods may affect product reliability.

THERMAL PERFORMANCE

Table 4.

Symbol	Description	Value[1]	Unit
θ_{JA}	Junction-to-ambient thermal resistance (still air) per JEDEC JESD51-2	24.1	°C/W
θ_{JMA}	Junction-to-ambient thermal resistance (1.0 m/sec airflow) per JEDEC JESD51-6	21.3	°C/W
θ_{JMA}	Junction-to-ambient thermal resistance (2.0 m/sec air flow) per JEDEC JESD51-6	20.0	°C/W
θ_{JB}	Junction-to-board thermal resistance (still air) per JEDEC JESD51-8	13.3	°C/W
Ψ_{JB}	Junction-to-board characterization parameter (still air) per JEDEC JESD51-6	12.8	°C/W
θ_{JC}	Junction-to-case thermal resistance	2.21	°C/W
Ψ_{JT}	Junction-to-top-of-package characterization parameter (still air) per JEDEC JESD51-2	0.23	°C/W

[1] Results are from simulations. PCB is JEDEC multilayer. Thermal performance for actual applications requires careful inspection of the conditions in the application to determine if they are similar to those assumed in these calculations.

ESD CAUTION

ESD (electrostatic discharge) sensitive device. Charged devices and circuit boards can discharge without detection. Although this product features patented or proprietary protection circuitry, damage may occur on devices subjected to high energy ESD. Therefore, proper ESD precautions should be taken to avoid performance degradation or loss of functionality.